Marott

~~SECRET~~/D

PAUL BETA SUBSYSTEM

ENGINEERING PROTOTYPE EVALUATION MODEL

(EPEM)

PART 0
FINAL REPORT

SUBCONTRACT NO. 029B25006

(PAUL)

31 OCTOBER 1968

52358-100-3 JAN 25 1969

~~1349-232~~

TABLE OF CONTENTS

TABLE OF CONTENTS (Continued)

LIST OF ILLUSTRATIONS

LIST OF TABLES

LIST OF REFERENCES

No.	
1.	Image Velocity Sensor Work Statement; (M&M) 4 December 1967
2.	Performance/Design and Product Configuration Requirements for Image Velocity Sensor; Specification No. EC-701A Rev. 5; (M&M) 4 December 1967
3.	Performance/Design and Product Configuration Requirements, Specification No. EC-701A Rev. 6; (M&M) 4 June 1968
4.	PAUL BETA Subsystem Engineering Prototype Evaluation Model (EPEM) Acceptance Test Procedure; (M&M) 13 September 1968
5.	Performance/Design and Product Configuration Requirements for Image Velocity Sensor; Specification No. EC-701B; (M&M) 31 July 1968
6.	BETA Subsystem Theoretical Response; (PAUL) 1 May 1968 .
7.	Cloud Detection Techniques Final Report, (PAUL) 16 October 1968
8.	BETA Subsystem Sensor Stress Analysis (Preliminary); (PAUL) 29 May 1968
9.	Technical Proposal; (PAUL) RFP 159; 28 June 1968

1.0 INTRODUCTION

1.1 SCOPE

This final report summarizes the work which was accomplished during the period 1 January 1968 to 30 September 1968, as defined in Reference 1.

The primary objectives of this program were:

(1) Design, develop, fabricate, test and deliver a BETA Subsystem Engineering Prototype Evaluation Model (EPEM).

(2) Provide necessary deliverable ancillary tools and test equipment to support engineering testing of the EPEM.

(3) Provide field test support for the BETA Subsystem Breadboard which was delivered to M&M in January 1968.

(4) Provide field test support, from October through December 1968, for the M&M evaluation testing of the EPEM.

Additional program objectives were:

(1) Perform related technical studies dealing with analysis, design, and performance characteristics of the BETA Subsystem.

(2) Provide a full-scale metal mock-up of the BETA Subsystem which simulates the external dimensions and form factor.

(3) Supply documentation reflecting the as-built condition of the EPEM.

1.2 SUMMARY OF PROGRAM OBJECTIVES

The objectives of this program were successfully accomplished with the delivery of the Engineering Prototype Evaluation Model (EPEM) and Ancillary Tester on 4 October 1968.

The EPEM, although a prototype model, reflects the prime hardware from a configuration and packaging standpoint and was fabricated using standard engineering shop processes and tolerances, such as would be employed for the prime hardware. Before delivery, the EPEM was subjected to a formal Acceptance Test which allowed the performance parameters to be evaluated in order to determine compliance with the performance requirements listed in Specification EC-701A Rev. 5 (see Ref. 2).

Close coordination was maintained with the contractor through weekly status reports, monthly status reports and technical direction meetings. Numerous technical reports discussing the analysis, design and performance characteristics of the BETA Subsystem and additional related studies dealing with scene parameters and tube characteristics were prepared and submitted to M&M. Overall program objectives and compliance are documented in the Detail Milestone Chart shown in Appendix A.

A full-scale metal mock-up of the BETA Subsystem simulating external dimensions and form factor was delivered in November 1967. No further effort in this area was required during the period of performance covered by this report.

Numerous trips were made to the contractors facility in order to support the test program for the BETA Subsystem Breadboard.

1.3 EPEM PERFORMANCE STATUS

ITEM	REQUIREMENT	PRESENT STATUS	COMMENTS
Dynamic Range	0-0.3 IPS	0-0.5 IPS	
Gain Factor	10 V/IPS	10 V/IPS	
Linearity			
Large Signal Region	Slope Limits (0.75-1.25)	1.0 to 1.1	
Null Region	Slope Limits (0.9-1.1)	0.924 to 1.078	
Saturation	5V/0.3 IPS	5V/0.3 IPS	
Noise & Bias (Null Region)	0.01 IPS (2σ)	0.02→0.04 IPS (2σ)	See section 2.3.4 for discussion of Noise Improvement
Frequency Response	1st Order Lag Over Output Range 0.001-0.25 IPS Break > 1 Hz.	First order lag to approximately 100 Hz.	See section 2.3.6 for frequency response discussion
Recovery Time After Saturation	In Saturation Over 2 Sec. Recovery ≤ 0.5 Sec.	0.30 Sec. (Max)	
	In Saturation 2 Sec. or Less, Recovery ≤ 0.1 Sec.	0.16 to 0.30 Sec.	See saturation recovery discussion in Sec. 2.4.3
Sub-Threshold Irradiance Signal	Flat Input of 4×10^{-9} wt/cm^2 per 10 Nanometer ($\Delta\lambda$) Over Range 400-900 Nanometers	Meets requirements	
Reliability	MTBF ≥ 10,000 Hrs.	15,500 Hrs (M&M computation)	
Warmup Time	≤ 3 Min.	13.72 Sec.	
Input Power			
Average	< 25 Watts	25 Watts	
Peak	< 50 Watts	29.5 Watts	

SECRET/D

SECRET/D

ITEM	REQUIREMENT	PRESENT STATUS	COMMENTS
Weight			
Sensor	≤ 14 Lb.	14.8 Lbs.	See Sec. 2.4.1.1 for sensor weight reduction discussion
System	≤ 22 Lb.	22.7 Lbs.	
Space Envelope			
Sensor	Per Dwg. 711-03013	8.9 Dia. x 18.75	
Electronics Assy.	6x6x6 In.	6x5.25x6.75 In.	
CG of Sensor			
Distance from Mtg. Plane Center Line	Within 0.25 In.	Within 0.1 In.	
Distance from Image Plane	≤ 7.25 In.	7.23 In.	
Thermal Dissipation			
Head	Design Goal < 3 Watts	8.9 Watts	See Sec. 2.4.2 for voltage reduction discussion
Generated Disturbances			
Vibration (During Exposure)	≤ 3.0 In.-Oz. (Any Axis)	None	
	≤ 0.01 Lb. Axial Force (Any Axis)		No moving parts in BETA Subsystem
(During Slew)	2X Above		
Resonance	> 50 Hz.		
Acoustic Noise	Per SAFSL 10003 Page 21		
Low Contrast	See Fig. 2.3.7-1	See Fig. 2.3.7-1	See Sec. 1.4.1.3 for low contrast performance improvement

SECRET/D

SECRET/D

1.4 PERFORMANCE IMPROVEMENTS & REQUIRED ADDITIONAL INVESTIGATIONS

1.4.1 PERFORMANCE IMPROVEMENTS

As a result of evaluation testing and BETA Subsystem studies performed during this program, three major performance problem areas were identified. These were:

(1) Dynamic Null,

(2) Low Contrast Performance,

(3) Signal-to-Noise Improvement.

1.4.1.2 DYNAMIC NULL

The first problem area - dynamic null - was the subject of considerable investigation. The investigation approach and conclusions reached are discussed in section 3.1.1. Briefly summarized, the conclusions state that the dynamic null rates obtained from both PAUL and M&M simulators are due to the increased field-of-view of the simulators and are approximately ~~70 times~~ greater than the rates corresponding to real-case geometry. The dynamic null problem was, therefore, adequately explained and is not considered to be a performance problem area in the final mission since the anticipated rates are below the specified threshold requirements.

WRONG

1.4.1.3 LOW CONTRAST PERFORMANCE

Figure 2.3.7-1 shows the EPEM performance evaluated for various contrasts over the required average illumination range. As can be seen from Figure 2.3.7-1, performance was not obtained over the total required rectangular area with the deficient area being high illumination - low contrast combinations in the lower right-hand corner of the rectangle. The limiting factor in the ability of the BETA Subsystem to perform with low contrast images is that of adequately storing (writing) the modulation content of the scene. Clearly, satisfactory system performance cannot be obtained unless initial storage of the image is enhanced. Methods are available, however, which will allow image modulation enhancement. These are:

(1) Write exposure control based on image modulation content,

(2) Spectral filtering and modified photocathode response.

1.4.1.3.1 WRITE EXPOSURE CONTROL BASED ON IMAGE MODULATION CONTENT

A method of optimizing the stored image is to first analyze the input image and then allow the write mode of operation to be

controlled so as to store a prescribed charge pattern sufficient to assure satisfactory operation. This can be done by dissecting the input image and analyzing the image content for modulation amplitude. The image dissection can be accomplished in approximately 5 milliseconds by using a storage mesh containing a small aperture (5-10 mils) at its center and deflecting the electron image across the aperture by means of a ramp input voltage applied to the deflection yoke. The resultant modulation would then be available, through the AC coupling at the sensor tube output, as a direct measurement of illumination vs. position in the input image. Comparison of the dissected output to the average value of illumination received by the sensor (photocathode current) would provide a direct measurement of the input scene contrast. The write exposure would then be controlled to optimize the stored image, based on the tube write time constant, and the tube storage mesh bias would then be automatically adjusted to center the stored modulation on the tube transconductance characteristic curve.

This technique of write exposure control would require the addition of some electronic circuitry to the present system and would increase the recycle time approximately 5 msec. However, the increased capability of the BETA Subsystem in analyzing and determining whether the input image content is acceptable prior to completing the operating cycle could result in a net saving in time when the input imagery is determined to be unacceptable for system operation.

The full potential of this technique of analyzing the input image cannot be fully explored until the input imagery characteristics are fully defined. However, it clearly lends itself to a sophisticated variable exposure control which will significantly improve the system performance with low contrast scenes. It is recommended that an investigation into the variable exposure control using the aforementioned technique be undertaken immediately in order to determine the amount of improvement possible in system performance.

1.4.1.3.2 SPECTRAL FILTERING AND MODIFIED PHOTOCATHODE RESPONSE

Low contrast performance can be improved by incorporation of spectral filtering used to reduce transmission for areas of the

illumination spectrum containing poor contrast. Additional low contrast performance improvement can be obtained by modification of the photocathode response so as to allow optimum matching of the sensor tube sensitivity to regions of the illumination spectrum containing the highest modulation to total illumination ratios. The approaches of spectral filtering and modified photocathode response can be employed since the present EPEM performance at minimum illumination exceeds the requirements of EC-701A Rev. 5. The minimum illumination requirements of EC-701A Rev. 6*are relaxed from Rev. 5: 0.028 ft-candles and 0.006 ft-candles, respectively. The present low-light level performance, which is more than sufficient for Rev. 6 requirements, in addition to higher expected photocathode sensitivities and further write exposure reduction due to increased storage mesh thickness, if required, allow the trade-offs of low-light level performance for spectral filtering to be made.

Based on investigations conducted during this program, it appears that the relatively poor contrast contained in the illumination spectrum region of 400-600 nanometers is low compared to the 600-1100 nanometer region and is probably due to atmospheric scattering effects. Effectively, the illumination in this blue region of the spectrum would lower the low contrast performance of the BETA Subsystem. With the illumination received below 600 nanometers filtered out and the photocathode modified to obtain the optimum match between received illumination spectrum and photocathode response, the low contrast performance would be significantly improved. Further investigation is required to identify the regions of the illumination spectrum which allow optimum modulation content to be obtained for all sun angles and with different scene content. It is recommended that a program be initiated to investigate these spectral illumination conditions.

1.4.1.4 SIGNAL-TO-NOISE IMPROVEMENT

As shown in Table 2.3.4-1, the total noise and bias error for PAUL #1 scene at 0.05 μa photocathode illumination level was 0.0394 ips and at 0.40 μa was 0.0183 ips, both of which are larger than the required value of 0.01 ips for total noise and bias error. Approximately 50% of the total noise figure for each of the X and Y

*See Ref. 3.

channels was contributed by periodic frequencies, the most predominant of which occurred at 57 Hz. Investigation is continuing to determine the cause of the relatively large periodic frequency content at 57 Hz. noted during EPEM acceptance testing and tests will be conducted using the PAUL breadboard unit. These tests will involve both subsystem and individual circuit frequency response data to determine if any non-linearities are present in the system and electronic filtering techniques to determine if a generating source is introducing the periodic energy. Determination of periodic frequency content will necessarily involve investigation of system packaging, signal routing, cross-talk between channels, shielding and power return terminations.

After the periodic frequency reduction is obtained, several system-oriented techniques for further random noise reduction are available. These techniques allow signal-to-noise improvement to be obtained as explained in the following paragraphs.

1.4.1.4.1 ADAPTIVE CONTROL

The previous discussion in section 1.4.1.3 concerning low contrast performance improvements use techniques which allow signal-to-noise improvement since image modulation enhanced by write exposure control and spectral filtering with modified photocathode response both result in increased signal level values.

Use of the information obtained by analyzing the input imagery can also be applied to optimizing the system response to the particular image parameters received by the BETA Subsystem. With the input imagery parameters known, and by using the fact that the image power spectral density and autocorrelation functions are Fourier Transform pairs, the subsystem gain and dynamic response can be controlled so as to obtain optimum performance for any image thus improving the overall signal-to-noise ratio of the subsystem. Thus, the subsystem could easily be made an adaptive system by optimizing its performance over a wide range of input image parameters. If desired, the BETA Subsystem could continually analyze the input imagery and, if sufficient information is not present for satisfactory operation, the subsystem would prevent the operating cycle from being initiated until the input imagery content would allow satisfactory operation.

It appears that the technique of analyzing the input imagery could provide information for the compensation of rates being sensed which are displaced from the center of format. Further study of this potential compensation is required; however, it appears that information derived by image dissecting could be used to bias the sensor tube such that image "slicing" occurs and only that portion of the image which would indicate the velocity at the center of format would be used by the system.

The similarity between the image dissecting technique using the sensor tube and that presently being used to obtain data for use in deriving the Wiener Spectrum for various scenes is evident. Therefore, it is recommended that a study be undertaken to ascertain the equivalent Wiener Spectrum for selected images obtained using the sensor tube. A meaningful correlation between Wiener Spectrum data obtained to date and the BETA Subsystem performance with various scenes could thus be obtained. A significant side benefit from this effort would be a better understanding of how the scene input parameters affect the subsystem performance.

1.4.1.4.2 FIXED RECYCLE TIME

Use of a fixed recycle time in which the verification and lock-on time of the BETA Subsystem operating cycle are controlled for a fixed time increment, would allow improvement in signal-to-noise ratio by a faster periodic updating of input information. The BETA Subsystem recycle command is presently determined only by the track verify circuit. Although the quality of the match signal determined by the track verify circuit is based on a comparison of 2 kHz, 1 kHz and noise content, the sensitivity of track verification is, by necessity, based on the average weighting of match frequency and noise content for a wide variety of scene parameters. Certain scenes may contain image content which can result in a match signal, satisfying the average requirements imposed by the track verify circuit, but whose rate indication may be questionable due to image slicing effects, shading, scale factor changes and low contrast conditions. A fixed recycle time, used in conjunction with the track

verification circuit would significantly minimize the probability of operation in instances where the correlation curve would be considered marginal by allowing the input image to be periodically restored allowing maximum useage of updated information to be realized.

1.4.1.4.3 MAGNETIC ZOOM

Incorporation of a magnetic zoom capability in the BETA Subsystem will allow compensation to be made for image scale changes as a function of line-of-sight. Although the scale factor and shading effects have been determined to be in the order of 70 times less than obtained in laboratory simulators, the technique of magnetic zoom will allow a further increase in signal-to-noise capability by image scale compensation. The implementation of magnetic zoom can be achieved by a modification of the focus coil windings in which the magnetic focus field would either minify or magnify the live image with respect to the stored image as a function of stereo angle. The exact amount of magnetic zoom will be determined by the average value of the cross-track and along-track compensation required as a function of the line-of-sight angles involved.

1.4.2 REQUIRED ADDITIONAL INVESTIGATIONS

1.4.2.1 GENERAL

A summary of the related study effort for this program is summarized in section 3.1 for three general categories:

(1) BETA Subsystem Analysis and Performance Parameters
(2) Sensor Tube Operation and Parameters
(3) Scene and Illumination Characteristics

For some studies, the effort undertaken on this program was, by definition, preliminary and further studies were anticipated in following programs to complete the effort. During the normal course of investigation related to the study objectives of this program, potential areas of improvement were identified, which, could not be completely investigated and still satisfy the primary study objectives. Additional investigations on following programs will be necessary to evaluate compliance with, and determine the effects of the revisions made in EC701 Rev. 6. The following sections describe the required additional areas of investigation and are subdivided into the following categories:

(1) Studies directly supporting future design effort,
(2) Studies involving evaluation of trade-offs in future design effort,
(3) Error analysis,
(4) Cloud obscuration.

1.4.2.2 DESIGN EFFORT SUPPORT STUDIES

1.4.2.2.1 CORRELATION MATCH POINT

A preliminary effort on the Correlation Match Point Effects study was started on this program. Basic concepts and a basic understanding of the effects of the image correlation match point effects on BETA Subsystem performance as a function of look angle were obtained. Refinements of the basic concepts and a complete evaluation of the image correlation match point effects on the determination of the velocity at the center of format remain to be completed. This study will involve analytical and experimental investigations of the effects of various scenes, with known correlation match points, on the BETA Subsystem performance.

1.4.2.2.2 ILLUMINATION SPECTRUM EFFECTS

The Illumination Spectrum Effects study will involve experimental and analytical evaluations in order to determine the effects of the revised illumination spectrum defined in EC-701A, Rev. 6 on BETA Subsystem performance. This study will include the determination of the effects of different atmospheric conditions as well as various sun angle and look angle effects on Subsystem performance with respect to the illumination spectrum.

1.4.2.2.3 OUTPUT POWER SPECTRAL DENSITY INVESTIGATION

This investigation will analytically and experimentally evaluate the output power spectral density with respect to the revised requirements of EC-701A, Rev. 6. The task is a continuation of the one started on this program. The additional required effort in this area will be to update the PSD computer program to be compatible with the revised specification and evaluate the updated BETA Subsystem design when it is available. Collaboration with M&M engineering will be required to properly update the computer program.

1.4.2.2.4 DYNAMIC RESPONSE INVESTIGATION

The Dynamic Response Investigation effort consists of developing the analytical transfer functions for the various functional blocks within the BETA Subsystem. A comparison of the theoretical block diagram with experimentally obtained data will be made in order to verify the theoretical work. The results of this study will aid in understanding and possibly improving the present system implementation.

1.4.2.3 TRADE-OFF STUDIES

1.4.2.3.1 DYNAMIC RANGE VS. ACCURACY

The Dynamic Range vs. Accuracy study will be primarily oriented toward defining and evaluating the trade-offs involved in changing the BETA Subsystem dynamic range to improve the accuracy of the system. Revised requirements for scaling and hence the dynamic range appear in

EC-701A, Rev. 6. These requirements will be evaluated and then the trade-off portion of the study will follow.

1.4.2.3.2 DYNAMIC RESPONSE VS. ACCURACY

This study will evaluate the revised requirements of EC-701A, Rev. 6 with regard to the BETA Subsystem response and identify and evaluate the trade-offs involved in improving the system accuracy by modifying the dynamic response. Experimental support for this study will be provided by the operation of a BETA Subsystem breadboard on the PAUL simulator.

1.4.2.3.3 LINEARITY VS. ACCURACY

The trade-offs involved in improving system accuracy at the expense of linearity will be identified and evaluated during the course of this study. Experimental evaluations of the possible trade-offs will be included.

1.4.2.3.4 POWER VS. WEIGHT VS. ACCURACY

A trade-off study will be conducted to identify and evaluate methods of improving accuracy by possible increases in subsystem weight and power. Experimental evaluations of the recommended trade-offs will be made, as well as analytical evaluations.

1.4.2.3.5 HIGH AND LOW FREQUENCY TIME SHARE OF LIGHT WITH THE VISUAL OPTICS VS. ACCURACY

The improvement in system accuracy will be investigated with respect to obtaining a higher input illumination level by time sharing the light made available to the visual optics. Providing additional light during periods of low light level operation clearly will improve the BETA Subsystem performance but possibly this light could be provided at a high frequency rate which would not appreciably deteriorate either the subsystem or the observers image and improved performance could be obtained without undue compromise of the observer. A complete analytical and experimental investigation of this mode of operation is planned.

NO! NOT FEASIBLE

1.4.2.3.6 ACCURACY VS. IMAGE LUMINANCE

The effects of variations in scene luminance on system accuracy will be investigated both analytically and experimentally. Both uniform and non-uniform luminance variations will be considered involving various atmospheric conditions and sun and look angles.

1.4.2.4 ERROR ANALYSIS

An error analysis of the BETA Subsystem will be conducted encompassing all error contributors from the input imagery to the output signals. Experimental verification of the analytical study will be made where practical.

1.4.2.5 DYNAMIC PERFORMANCE MODEL STUDIES

The objective of this analytical and experimental study will be to complete the development of a math model of the BETA Sensor. The model will be implemented in the form of a digital program for the IBM 360 (S40) computer, in order to provide an efficient and flexible capability to predict the output signal performance characteristics as a function of changes in either the input image parameters or in the sensor internal component parameters.

During this program, a separate study was performed to develop the techniques required for mathematically specifying the input optical image. This preliminary effort primarily concerned the evaluation of computer generated synthetic images, to identify the scene parameters which significantly influence the sensor correlation response. Generally, these special images were mathematically specified by a tabulation of the transmissivity and color at each individual point across the entire format.

Also during this program, a separate study was performed to develop the techniques required for mathematically specifying the performance of the BETA Sensor tube. Emphasis was restricted to this particular component of the sensor, since the tube operation represents a complex inter-relationship between many individual physical responses. This preliminary effort identified the responses that were significant to the model, and defined appropriate mathematical expressions. Generally, the tube model was formulated on the basis of synthetic input imagery that could be specified on a point-by-point basis.

On following programs, these two investigations will be continued, but they will be integrated into a single program to develop a sensor math model. This reflects the need to provide a marriage between the response function of the sensor and the excitation function of the input image. Accordingly, future efforts will primarily concern an effort to specify complex actual input imagery in a mathematical form that can be accepted by the sensor model, and to adapt the sensor model to insure full accommodation of the input stimulus. To achieve a manageable model, an image specification technique other than a point-by-point tabulation will be required; i.e., one which can combine all the significant image characteristics into a relatively simple mathematical expression.

To develop such an expression, both analytical and experimental studies will be performed. The laboratory effort will include the scanning of image samples with a microdensitometer to determine the spot size (resolution) and the scanning patterns (% coverage) that are required for adequate specification. An attempt will be made to find suitable combinations wherein the data obtained from relatively few scans, or from averages obtained by non-spot aperatures (e.g., slits), is shown to be sufficient. Tests will also be performed with coherent and non-coherent optical processors to determine whether data extracted from the frequency transform plane or from the autocorrelation response will be sufficient. It is likely that data obtained from a reasonable combination of these various sources will be required for a comprehensive specification of the image characteristics, and that machine processing of this data will be required to generate the corresponding mathematical expression for the model input stimulus.

The analytical effort concerning image specification will provide the equipment and measurement parameters to be examined experimentally, based on the image characteristics which are known to influence the correlation response. This effort will also provide the programming necessary to process the resulting data. The effort will not include a specific effort to establish the nominal physical characteristics of terrain imagery received at a spaceborne sensor. The effort will,

however, include a study to determine if these nominal characteristics, if available, could be used to adequately specify the model input stimulus. Such summary characteristics are spatial frequency distribution, spectral distribution, etc. will be considered.

The image specification study will be closely coordinated with the development of the sensor model, to insure that the expressions for the input stimulus are mechanized in a form that can be readily accommodated by the model. Likewise, the prediction performance that results from trial exercising of the model will be evaluated to identify deficiencies in the image specification and to conceive necessary improvements or allowable simplifications.

The effort to develop a mathematical model of the BETA Sensor will, as previously mentioned, include modification of the model form in order to accept input expressions that fully describe complex actual terrain images. In addition to this, the study will include the general improvement and refinement of the expressions used to describe the individual physical responses and their interactions within the sensor tube. The model will also be expanded to include the electronics external to the tube, as required to fully describe the output signal characteristics under null and dynamic conditions. Expressions for noise and non-linear responses will also be included.

Also, a significant effort will be expended to program the 360 computer as defined by the math model, and then to exercise the computer in such a manner as to isolate the deficiencies. For this evaluation, actual sensor output signal characteristics will be generated from comparison with the model results by performing appropriate tests with the Princess Sensor and Laboratory Simulator.

1.4.2.6 CLOUD OBSCURATION STUDY

The objective of this analytical and experimental study will be to determine how specific cloud and terrain parameters influence the intended performance of the BETA Sensor, and to determine the characteristics of sensor signals that are selected as indicative of cloud obscuration. This will be a logical continuation of a corresponding effort initiated during this program. As such, the proposed effort will primarily concern the refinement of image parameters, obscuration simulation, test procedures, and data evaluation.

The study will include a continued evaluation of engineering data concerning typical cloud characteristics that is available from this and other programs. This information will be used to develop obscuration simulation techniques which provide more realistic parameters. The servo-driven image fixture, the BETA Sensor, and the Laboratory Simulator will be used to experimentally determine which obscuration models prohibit "in-spec" performance when used in conjunction with a variety of typical terrain scenes. This data will be compiled in a form to show the probability of successful performance as a function of the type and degree of obscuration.

Also as part of these tests, selected signal points within the sensor will be monitored. This data will be evaluated to determine the nominal characteristics of these signals as a function of the obscuration parameters. These characteristics will be analyzed, in turn, to develop computer processing techniques capable of automatically indicating the type and degree of obscuration. Analysis or trial computer runs will be performed to identify obscuration conditions which can result in ambiguous indications, or in errors of commission or omission.

Refinements in signal measurement techniques and/or alternate processing techniques will be evaluated, as required to minimize these deficiencies.

At the conclusion of this study, it is anticipated that the obscuration conditions which can prohibit satisfactory performance of the BETA Sensor will be specified. Likewise, the signal measurement and signal processing techniques required for an automatic indication of obscuration conditions will be defined in sufficient detail to adequately determine the influence of this capability on the mission effectiveness.

2.0 ENGINEERING PROTOTYPE EVALUATION MODEL (EPEM)

2.1 THEORY OF OPERATION

2.1.1 FUNCTIONAL

Figure 2.1.1-1 shows a block diagram of the PAUL BETA Subsystem and the table in Appendix B compares the functional differences between the EPEM and the on-site BETA breadboard subsystem (Princess I). Following is a discussion of the subsystem operation.

In order to obtain image rate information, the system centers around a special storage tube. This tube requires three modes of operation:

(1) A "write" mode, at which time the initial image position is stored as a two-dimension charge pattern and during which no output can be given.

(2) A "read" mode, wherein correlation of the input image and the previously stored reference is performed, and during which the sensor output is enabled.

(3) An "erase" mode, wherein the previously stored reference charge pattern is removed from the storage mesh, and during which the sensor output is inhibited.

During the write mode, an optical image is stored as a charge within the tube by electron secondary emission of the storage mesh.

During the read mode, a switching sequence is enabled to the tube elements to reduce the electron velocity so a non-destruct readout can be performed. Thus, for the single write sequence, many non-destructive comparisons can be made before signal degradation occurs and a new write sequence is required. Before a new image can be stored it is necessary to erase completely the previously stored image. This is accomplished by properly biasing the tube and flooding the storage mesh with a uniform electron bundle.

The data stored in the tube is fixed on an x-y plane. The incoming optical image produces an electron bundle within the tube which is modulated a small amount by field deflection in the coils around the tube and an area match yields a maximum output when the input and stored images are superimposed. Closed-loop characteristics of the BETA Subsystem maintain the image superposition in a best match condition by deflecting the field around the tube and displacing the incoming image.

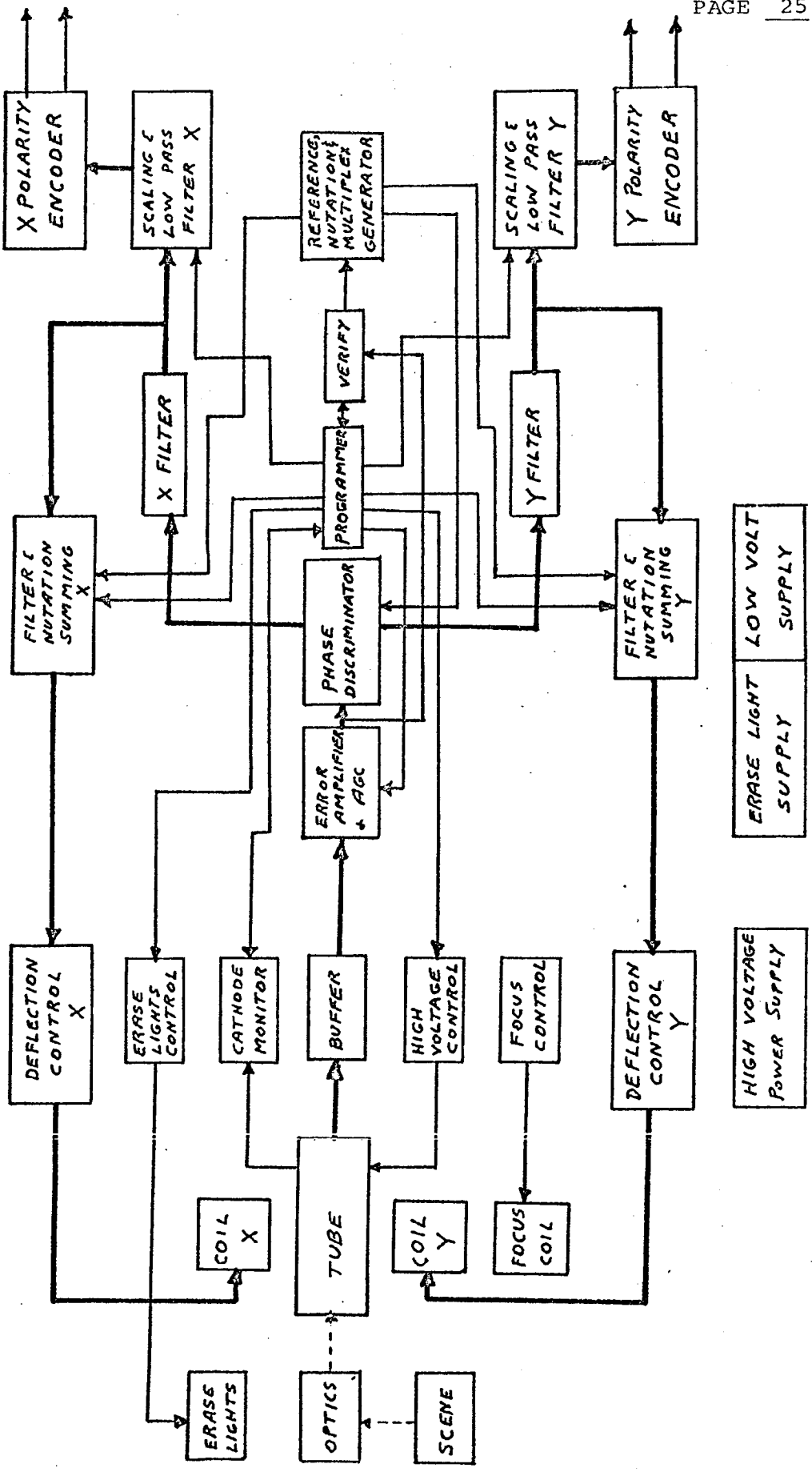

Figure 2.1.1-1. PAUL BETA Subsystem Block Diagram

The incoming image is nutated alternately in the x and y directions by a one kilohertz sine wave, switched at a 500 Hz rate. The output data is thus a complex, multiplexed signal which is synchronously demodulated to separate x and y output channels. During a closed-loop match condition, this signal appears as a full-wave rectified sine wave. Under normal conditions this signal may vary from one millivolt peak-to-peak to 150 millivolts peak-to-peak depending on the image and, at the tube output, is referenced to a 2,000V DC level.

The output signal is coupled through a buffer amplifier to ground level where it is amplified and held to a 3 volt peak-to-peak level without distortion or phase shift. To accomplish this, three stages of amplification are used which provide a common bandpass well in excess of an order of magnitude above and below the error signal frequency.

Since the signals are multiplexed, only a single channel of gain is required. However, to properly AGC the separate x and y data, there are two separate AGC amplifiers which are multiplexed synchronously into the feedback loop in one of the three stages.

The purpose of holding the error signal at a constant amplitude is to maintain a constant forward-loop gain and thus constant loop dynamics.

The fixed amplitude wave is then passed through the phase discriminator which reconstructs the match signal in a manner to obtain the least DC output for the best match. When the input image moves away from the stored image, the match signal becomes distorted. The phase discriminator determines the magnitude and direction to deflect the incoming signal in order to obtain the best match.

The correction signal, still multiplexed, is now separated by synchronous demodulation and sent to separate x and y filters for processing. Each filter is designed to produce two single lags, one at 60 Hz, the other at 210 Hz. The signal separation is accomplished prior to these filters to avoid smearing the x and y data.

Each of the nutation summing amplifiers has a DC input which is controlled by the output of a position integrator. The input to each of the integrators is the output from the corresponding x or y filter. By summing the nutation signal and the integrator output, the incoming image is deflected across the stored image maintaining the best match signal. When the incoming image is displaced away from the centroid far enough such that the integrator can no longer force the deflection to match, then the "saturation limiters" force an erase-rewrite mode. The new write will start with the stored image in the center of the tube and both integrators zeroed.

The closed-loop response maintains the optimum position match between the incoming image and the stored image. The integrator which maintains "position" must, by definition, have "rate" as its input. Rate inputs to the integrators are filtered by a 3.5 Hz filter and this relative DC output is scaled to provide the proper range of voltages for the input image rates encountered. This output is converted to provide a zero to plus five volt input to the analog to digital converter. The polarity bit will be used with the digital readout for negative excursions.

To insure that good rate information is being given and that the system is not lost during lock-on, a verification circuit is provided. The verification circuit monitors the match signal from the third error amplifier and compares the magnitude of the 2 kHz match signal to the magnitude of the 1 kHz off-match signal and the magnitude of the noise. If the ratio of 2 k to 1 kHz or the ratio of 2 kHz to noise is greater than a predetermined level, the verify circuit forces a recycle.

2.1.2 OPERATION SEQUENCE

The operating sequence is implemented in the following manner:

1. A 13 second warm-up interlock is enabled when power is applied.
2. At the end of warm-up, and if the input scene illumination level is greater than 0.035 μamps photocathode current, the system steps into the "standby" mode which indicates operational readiness.

3. If a "track command" is available, the system will step from standby without delay. Without a "track command" it will remain in the operational ready or "standby mode". Given the three primary "initial conditions": the 13 second warm-up, satisfactory illumination and a track command, the system will initiate an erase to prepare the tube and establish all initial conditions in the operating sequence.

4. The next sequence step is a "write" cycle which is dynamic with light intensity such that a low light causes a longer write period. At present, 0.1 μamps photocathode current requires a write time of 120 milliseconds.

5. When the write mode is satisfied, the tube is switched to the "read mode". For the first 112 milliseconds of the read mode, a stabilization and verification period is established. After 80 milliseconds of stabilization, the 3.5 cycle filter inputs are enabled to permit their stabilization before being placed "on line". The verification circuit is also enabled to permit an evaluation of the match.

   If, at this time, the verify circuit indicates a fail condition, the nutation amplitude is increased in an attempt to force a pass verify. 32 milliseconds is allowed after the increase in nutation to evaluate the new match signal. If the verify circuit still indicates fail, the system is forced into a recycle. If the verify output indicates a go condition, the system is ready to go into the lock-on mode. If, after 80 milliseconds, the verify circuit had produced a pass signal, the system would have waited 32 milliseconds more before going to the lock-on mode.

At the end of the 112 millisecond stabilization time, the position saturation monitors are enabled. Two clock pulses at a 2 kHz clock rate are permitted before the lock-on signal and output data are released to permit verify or saturation to operate prior to lock-on.

6. "Lock-on" consists of passing the verify test without limiting on the position or deflection coil drives. Otherwise, an erase mode is activated and a new cycle begun. A rate saturation is read out but does not force a recycle. During "lock-on" the verify circuit makes a continuous monitor of the quality of the match. Once in the "lock-on" mode, the system will stabilize and "match" the image until the deflection coils reach a limit or the verification indicates a degraded match signal. The system will continue to recycle and relock-on until the "track command" is removed or low input illumination is encountered.

7. There are two operational modes that will stop the system with the track command on: one is low input illumination, the second loss of power.

   (a) If low illumination is encountered, a low light indicator is activated to produce a system output subthreshold illumination indication and the system continues in lock-on until the next recycle. Recycle can be initiated by either the track verify circuit or a saturation command to the system. If this occurs, the system completes the erase mode and stops the clock.

   When the light again becomes available and if the track command is still on, it will erase again to clear the system and then continue cycling.

   (b) If power is dropped for less than one second the system will not go through warm-up. It will erase as the first step when power comes back on. If power loss is longer in duration, the system will "warm-up" for up to 13 seconds, erase and then continue operation.

2.1.3 BETA SUBSYSTEM RESPONSE

2.1.3.1 GENERAL

A simplified block diagram is shown in Figure 2.1.3-1 in which a single transfer function for the forward-loop terms and a single feedback loop transfer function is shown. The forward-loop transfer function from X_e to $\dot{X}_i$, consisting of a gain term and the dynamic portion, two lag frequencies, is:

$$\frac{\dot{X}_i}{X_e} = \frac{1100}{\left[\frac{S}{2\pi 99} + 1\right]\left[\frac{S}{2\pi 178} + 1\right]}$$

This expression combines the tube, buffer amplifier, error amplifier, AGC circuit, phase discriminator, and associated filter circuit responses. The feedback loop transfer function from $\dot{X}_i$ to X_f of $\frac{0.1}{S}$ includes the integrator, nutation summing network, deflection control amplifier, and deflection coil circuits.

The optics and tube response to the scene velocity input $\dot{X}_{in}$ to X_{in} are shown as a single block whose transfer function is $\frac{1}{2.8S}\frac{in}{in/sec}$. The scaling amplifier and low-pass filter from $\dot{X}_i$ to $\dot{X}_{out}$ has the following transfer function:

$$\frac{2.8}{\left[\frac{S}{2\pi 3.5} + 1\right]}$$

The single lag at 3.5 Hz is used to modify the overall loop response to obtain the desired characteristics. The 2.8 gain term is used to cancel the optical attenuation value of $\frac{1}{2.8}$.

2.1.3.2 OPEN-LOOP TRANSFER FUNCTION

Stability of the control loop can be determined from an open-loop Bode Plot of the forward and feedback-loop transfer functions.

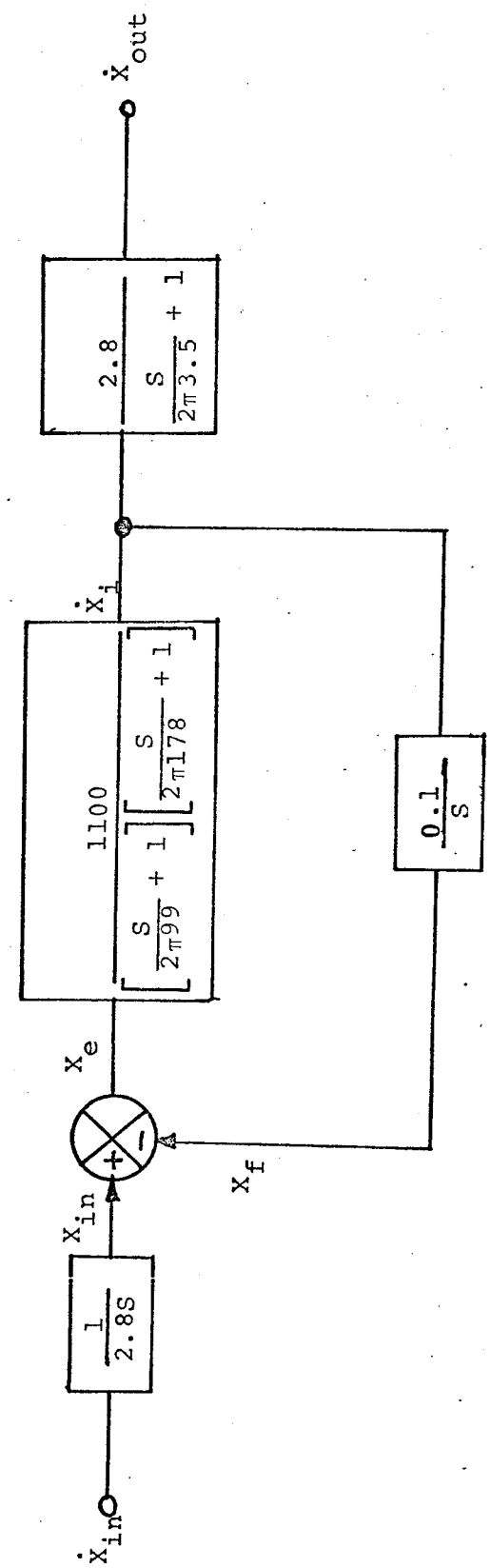

Figure 2.1.3-1. Simplified Transfer Function Block Diagram

Thus:

$$KGH(S) = \frac{110}{S\left[\frac{S}{2\pi 99} + 1\right]\left[\frac{S}{2\pi 178} + 1\right]}$$

The Bode Plot is shown on Figure 2.1.3-2 and indicates a cross-over frequency of 8 Hz. The combined gain margin of 23 db and phase margin of 75 degrees indicates a very stable control loop.

2.1.3.3 CLOSED-LOOP TRANSFER FUNCTION

The forward-loop transfer function KG(S), and the feedback transfer function H(S), can be combined to obtain a closed-loop transfer function

$$\frac{\dot{X}_i}{X_{in}} = \frac{KG(S)}{1 + KGH(S)}$$

Substituting values for KG(S) and H(S) from the loop portion of the simplified block diagram:

$$\frac{\dot{X}_i}{X_{in}} = \frac{\frac{1100}{\left[\frac{S}{2\pi 99} + 1\right]\left[\frac{S}{2\pi 178} + 1\right]}}{1 + \frac{110}{S\left[\frac{S}{2\pi 99} + 1\right]\left[\frac{S}{2\pi 178} + 1\right]}}$$

$$= \frac{1100\ S}{S\left[\frac{S}{2\pi 99} + 1\right]\left[\frac{S}{2\pi 178} + 1\right] + 110}$$

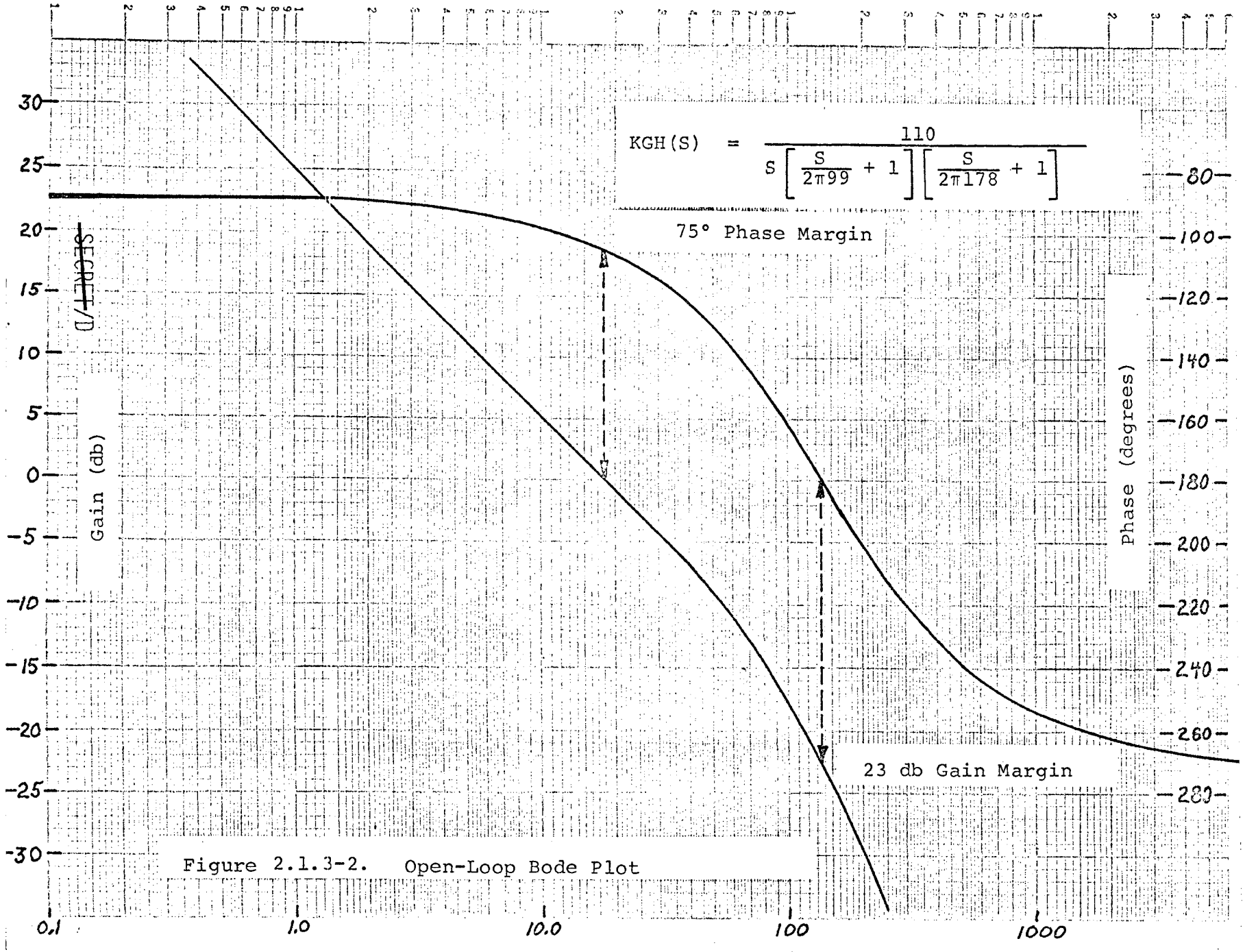

Figure 2.1.3-2. Open-Loop Bode Plot

For purposes of analysis, the optical scale factor $\frac{1}{2.8}\ \frac{\text{in.}}{\text{in.}}$ will be neglected in the determination of $\frac{\dot{X}_i}{\dot{X}_{in}}$ but will be considered in the overall BETA Subsystem transfer function $\frac{\dot{X}_{out}}{\dot{X}_{in}}$.

Solving for $\frac{\dot{X}_i}{\dot{X}_{in}}$ by multiplying through by

$$\frac{X_{in}}{\dot{X}_{in}} = \frac{1}{S}$$

gives

$$\frac{\dot{X}_i}{\dot{X}_{in}} = \frac{1100}{S\left[\frac{S}{2\pi 99} + 1\right]\left[\frac{S}{2\pi 178} + 1\right] + 110}$$

$$= \frac{1100\ (2\pi 99)\ (2\pi 178)}{S^3 + S^2\ [(2\pi)(99+178)] + S\ 4\pi^2\ [(99)(178)] + 110\ [(2\pi 99)(2\pi 178)]}$$

This cubic can be factored into the conventional form

$$\frac{\dot{X}_i}{\dot{X}_{in}} = \frac{10}{\left[\frac{S}{2\pi 30} + 1\right]\left[\frac{S}{2\pi 52} + 1\right]\left[\frac{S}{2\pi 195} + 1\right]}$$

To determine the overall system response, the equation for $\frac{\dot{X}_i}{\dot{X}_{in}}$ must be multiplied by the transfer function of the 3.5 Hz filter. The gain term of this filter cancels the attenuation term of the optics ratio.

$$\frac{\dot{X}_{out}}{\dot{X}_{in}} = \frac{\dot{X}_i}{\dot{X}_{in}}\left[\frac{1}{\frac{S}{2\pi 3.5} + 1}\right]$$

Therefore, the overall transfer function is

$$\frac{\dot{X}_{out}}{\dot{X}_{in}} = \frac{10}{\left[\frac{S}{2\pi 30} + 1\right]\left[\frac{S}{2\pi 52} + 1\right]\left[\frac{S}{2\pi 195} + 1\right]\left[\frac{S}{2\pi 3.5} + 1\right]}$$

and is shown plotted in Figure 2.1.3-3.

$$\frac{KG(S)}{1+KGH(S)} = \frac{10}{\left[\frac{S}{2\pi 30}+1\right]\left[\frac{S}{2\pi 52}+1\right]\left[\frac{S}{2\pi 195}+1\right]\left[\frac{S}{2\pi 3.5}+1\right]}$$

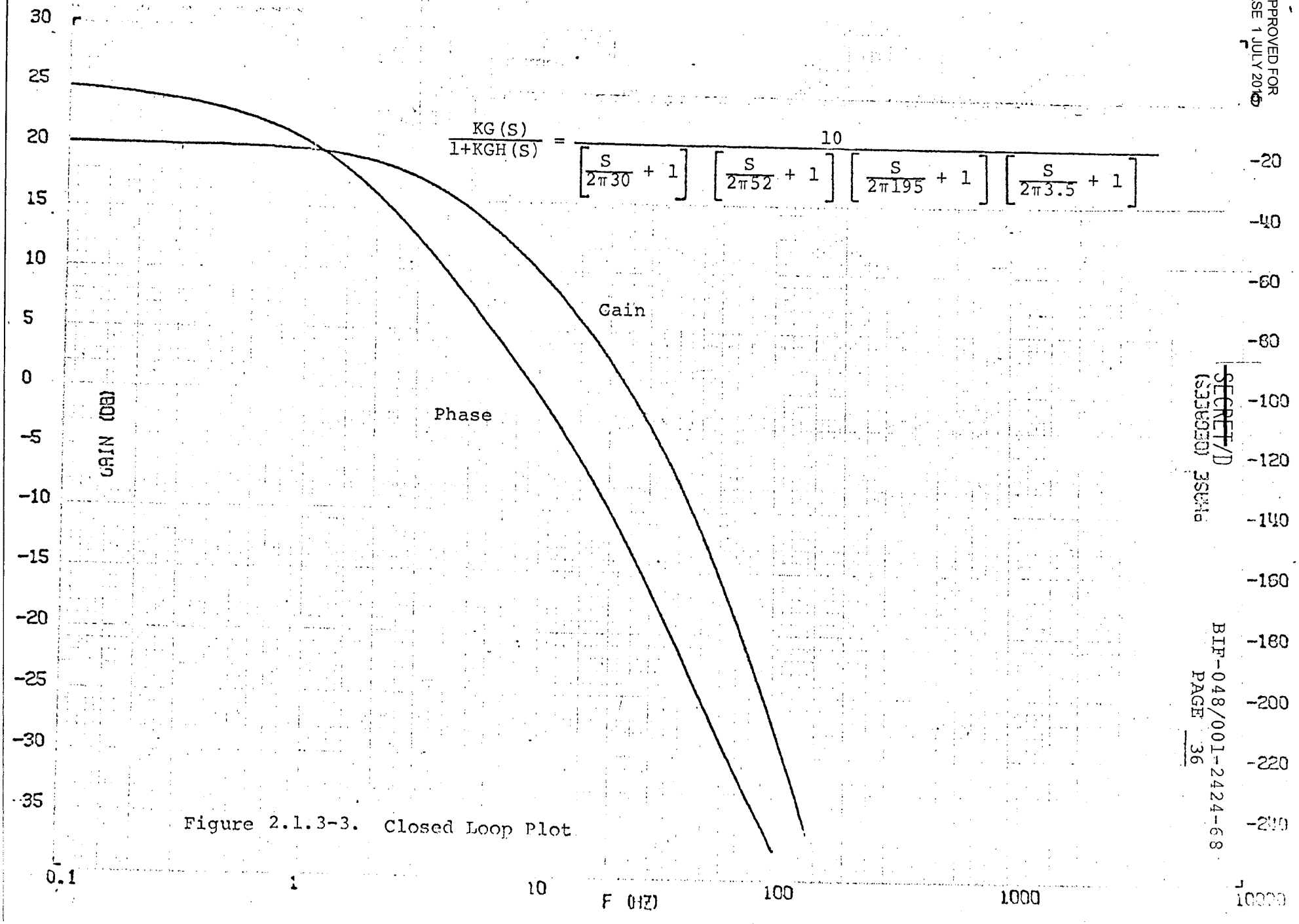

Figure 2.1.3-3. Closed Loop Plot

2.2 DESCRIPTION

2.2.1 SENSOR PACKAGE ASSEMBLY

Packaging Considerations

The following items are packaged in the Sensor Assembly:

(1) Storage tube and sleeve assembly,
(2) Deflection coils and support,
(3) Focus coil, support, and shield,
(4) Cathode contact ring and support,
(5) Erase lights and support,
(6) Hermetically-sealed electrical connector,
(7) Optics including field lens, helium barrier window, and relay lens assembly,
(8) Sensor body weldment and covers for electronics,
(9) Electronics requiring close proximity:
    (a) X and Y Deflection Control,
    (b) Erase Light Control,
    (c) Cathode Monitor,
    (d) Buffer Amplifier,
    (e) High Voltage Control,
    (f) Focus Control,
    (g) High Voltage Power Supply.

Arrangement of the above items into a complete sensor package required careful consideration of several factors before a final design could be realized. Included were environmental, reliability, maintainability and manufacturing requirements, even though the EPEM was not required to have passed qualification or production acceptance testing. The final design was predicated on the following conditions:

(1) Operational Conditions:
    a) Temperature range: -65°F to +160°F
    b) Shock: 35g half-sine wave for 2.6 millisecond duration
    c) Vibration: .01 g^2/Hz for 10 to 140 Hz; linear increase plotted on log-log scale from .01 to .035 g^2/Hz over 140 to 260 Hz frequency band; .035 g^2/Hz level from 260 to 1,200 Hz; -3 db/oct roll-off for 1,200 to 2,000 Hz frequency band

d) Pressure: 10^{-9} mm Hg min and 14.7 psi max.

e) Helium gas leak rate: Less than 10^{-9} cc/sec when tested in one atmosphere of Helium

(2) Accuracy: Since the assembly operates as an electro-optical device, a primary consideration of the mechanical design was to insure built-in accuracies so as not to compromise the electro-optical requirements.

(3) Reliability versus Serviceability: Primary consideration was given to reliability of design without sacrificing necessary serviceability requirements.

(4) Weight: The Sensor Assembly weight was 14.8 pounds.

(5) Manufacturing Requirements: The sensor package was designed to simplify the fabrication of parts such that excessive complex tooling or manufacturing techniques would not be required. The design was also based on making all assembly and subassemblies with a minimum of tooling and effort.

(6) Hermetic Sealing: Two methods of making the required hermetic seal were developed. A hermetically-sealed package is required due to the exposure of the package to a helium environment.

Package Description

Housing and Subassemblies

The following discussion describes the sensor package configuration which is pictured in Figure 2.2.1-1. Assembly and subassembly configurationsare also explained and the major subassemblies are shown in Figures 2.2.1-1 through 2.2.1-5.

Support for the tube is accomplished by means of a metal sleeve and elastomer interface. This combination maintains the mechanical

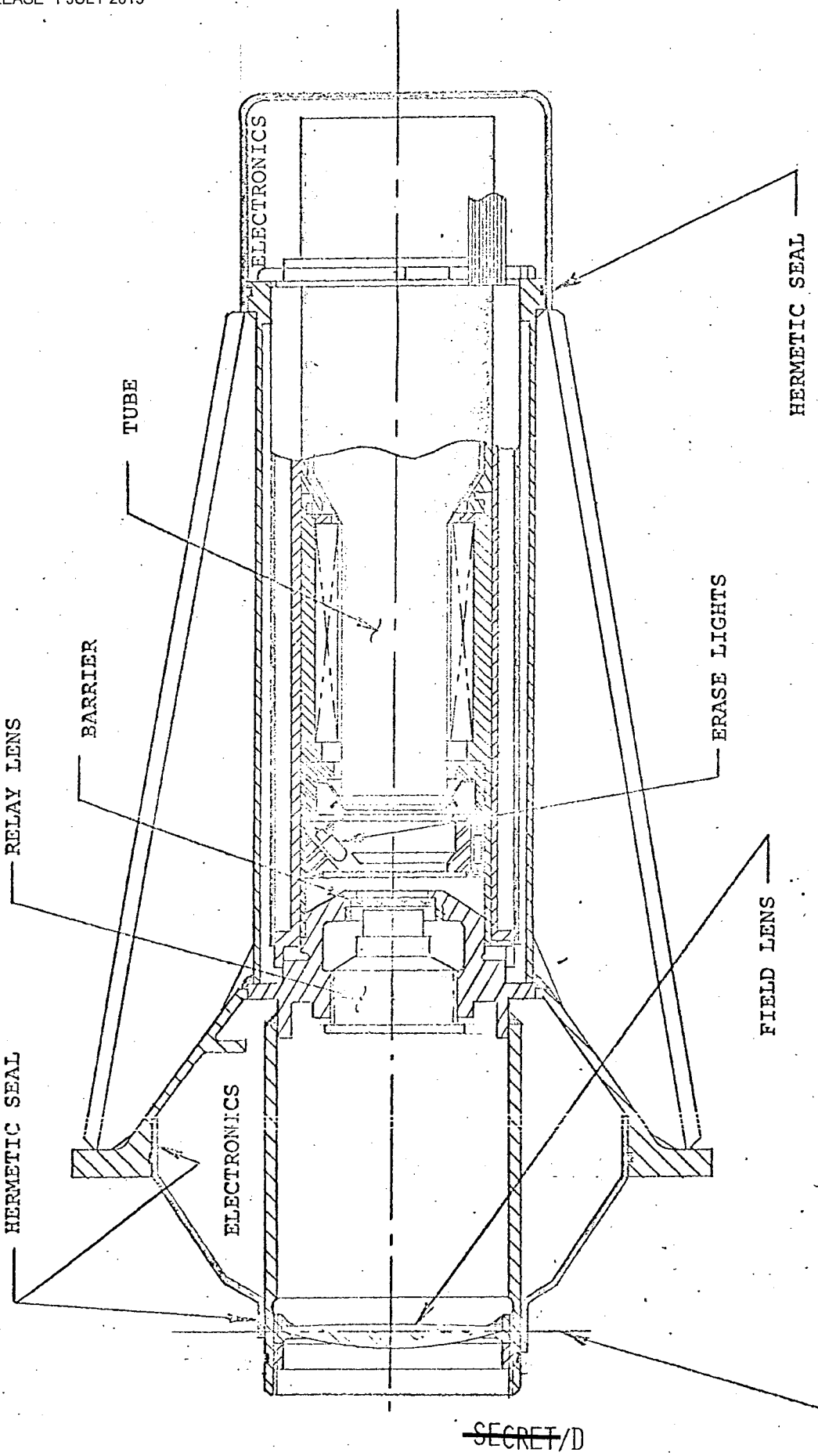

Figure 2.2.1-1. Sensor Assembly

support and alignment initially set up by special fixturing. The elastomer is cured in place and forms a dense, uniform interface between the tube and the sleeve. The sleeve positions the tube accurately in all axes and is locked in place at its final installation. This subassembly is shown in Figure 2.2.1-2.

Figure 2.2.1-3 shows the subassembly of the erase lights, photocathode contact ring, and contact ring support. This subassembly is actually the combination of two lesser assemblies - the erase lights and the contact ring assembly. The erase light assembly contains 16 selected neon lamps accurately located by fixturing and cementing in place. After addition of two printed circuit rings with leads and a resistor in series with each of the 16 lamps, the entire subassembly is assembled to the contact ring assembly by means of a fixture which establishes the correct axial relationship plus the required concentricity. The entire assembly is then potted.

The deflection coil form construction and assembly is governed mainly by the electrical requirements as is its physical position in relation to the tube. This form also accepts the erase lights, contact ring, and contact ring support. These items are then positioned in the focus coil form which has previously been wound with aluminum magnet wire in order to minimize the assembly weight. After positioning and potting all electrical leads in place, the magnetic shield is placed over the entire subassembly and epoxyed as shown in Figure 2.2.1-4. The deflection coil form is keyed to the focus coil form which can then be adjusted during checkout for the correct axial alignment.

The main body or housing is a welded assembly machined so as to maintain proper positioning and alignment of all sensor package subassemblies. In addition, this housing has an exhaust tube which is used after final assembly to evacuate and back-fill the sensor package with dry nitrogen. The tube is then pinched off in order to complete the sealing as shown in Figure 2.2.1-5.

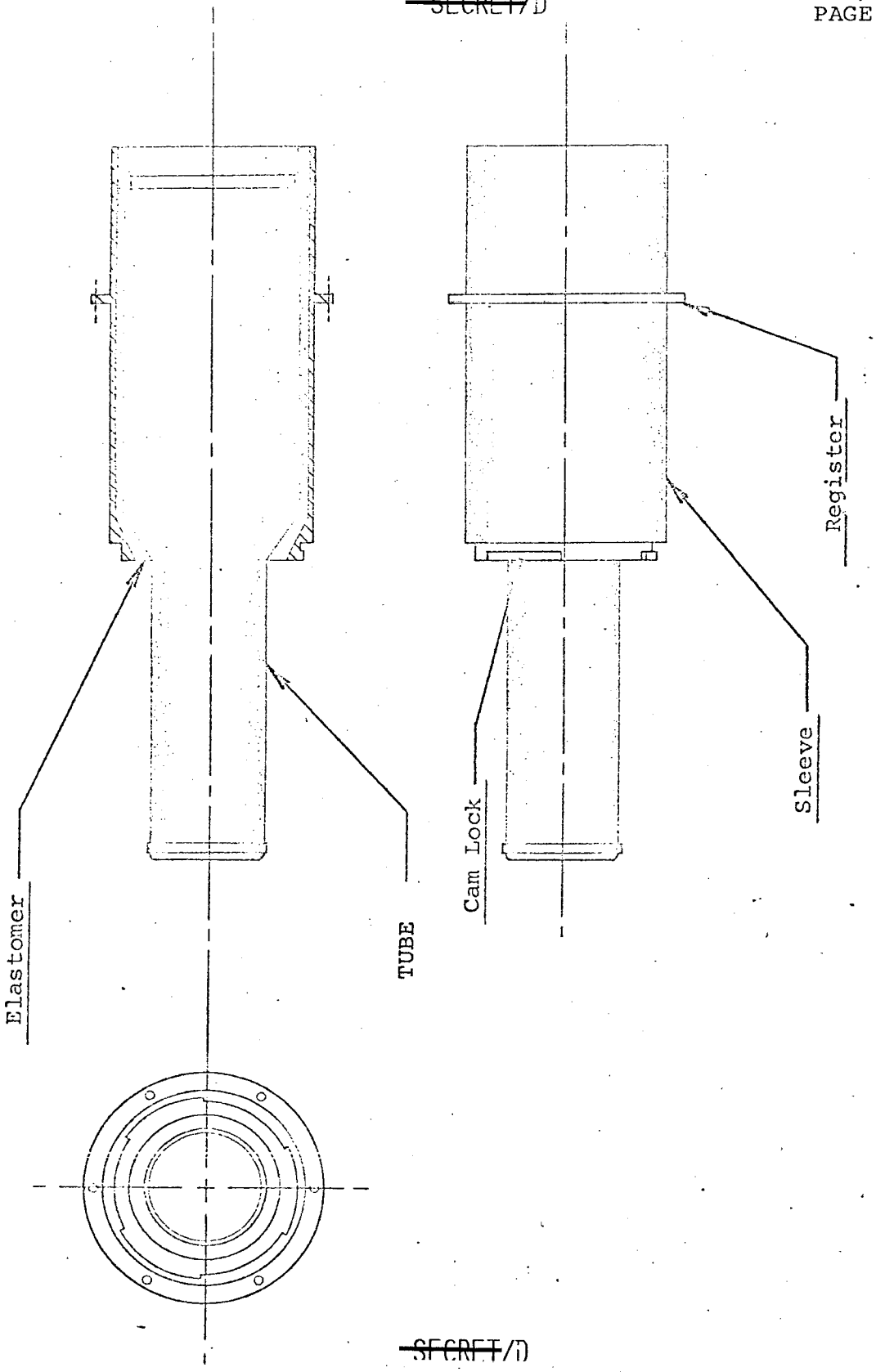

Figure 2.2.1-2. Tube Assembly

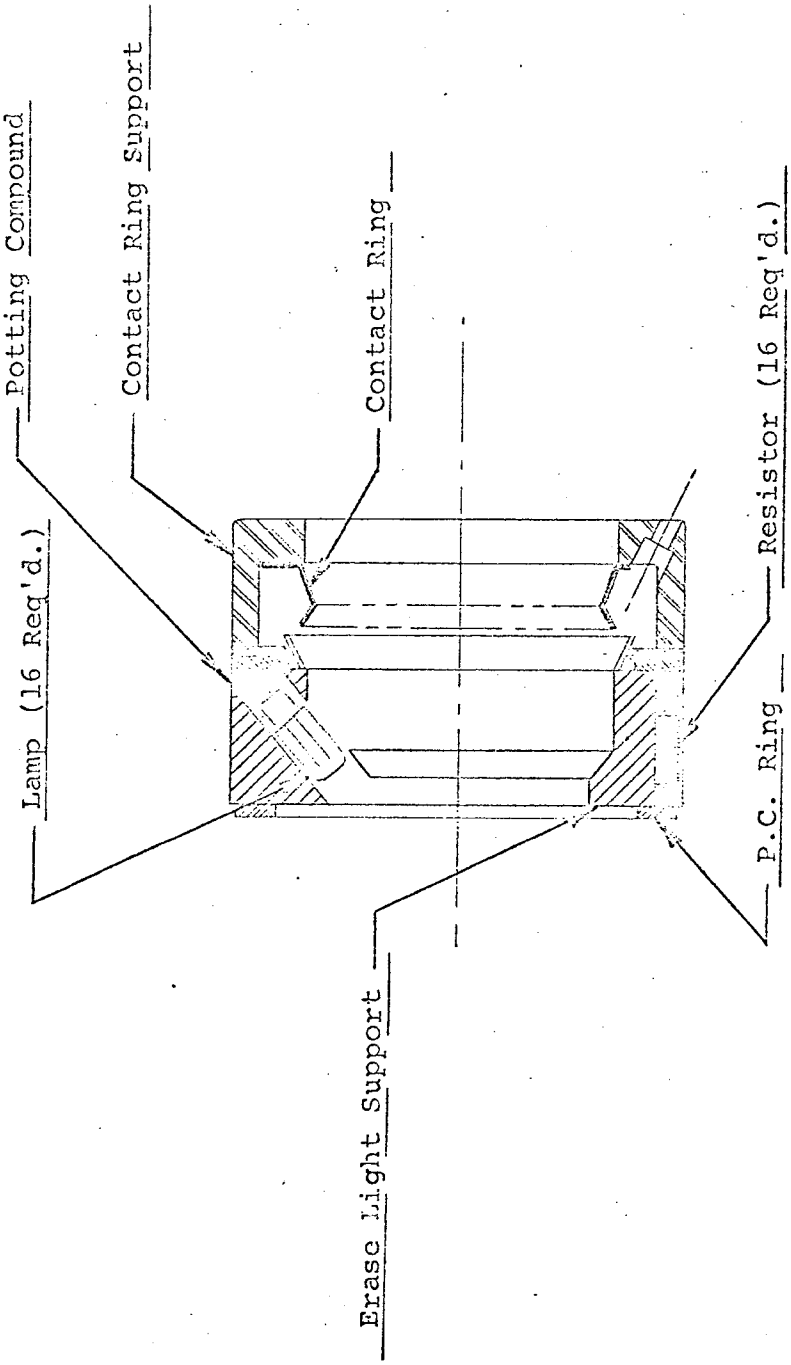

Figure 2.2.1-3. Erase Light and Contact Ring Assembly

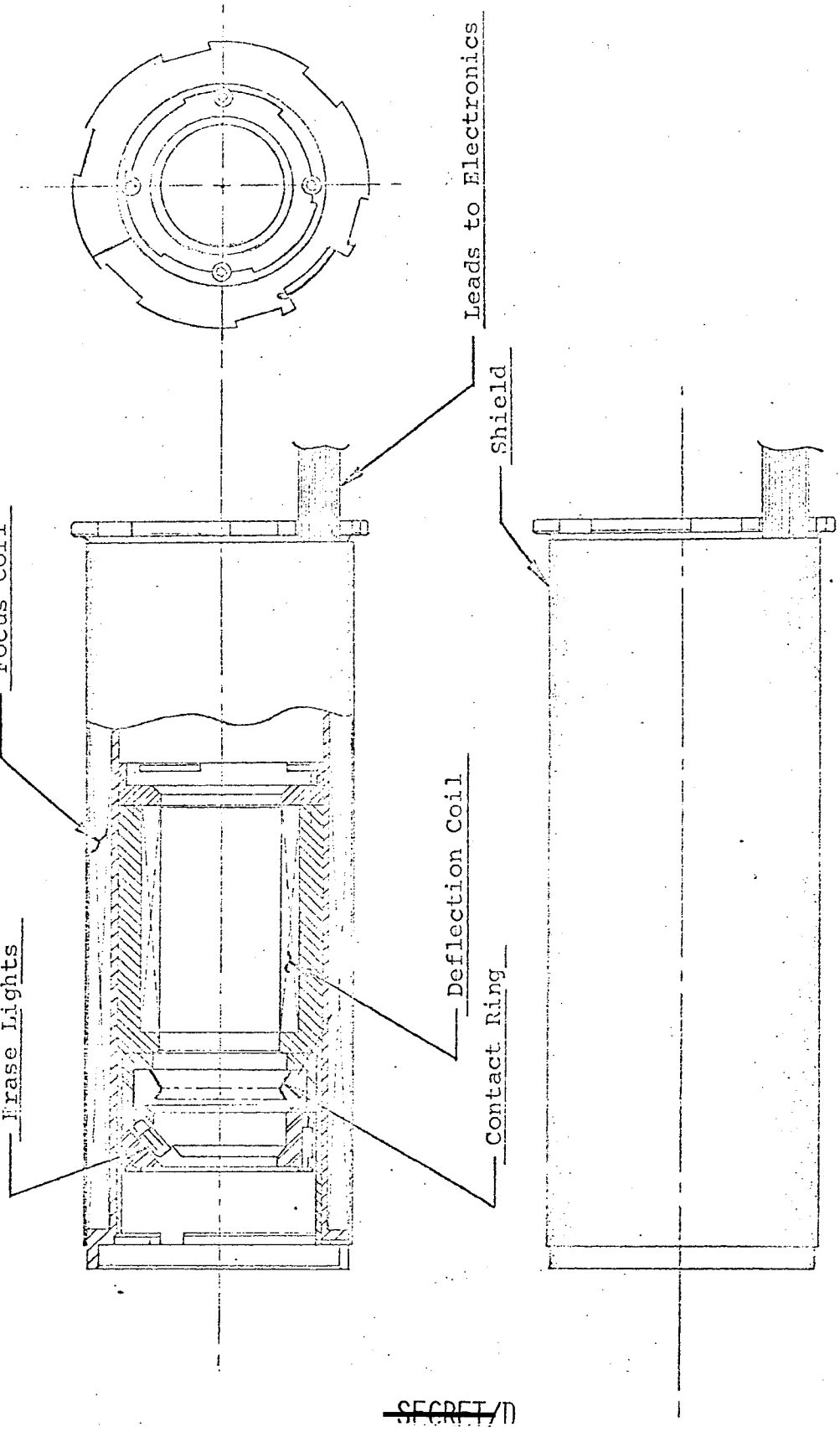

Figure 2.2.1-4. Subassembly of Erase Lights, Focus Coil, Deflection Coil, Contact Ring and Shield

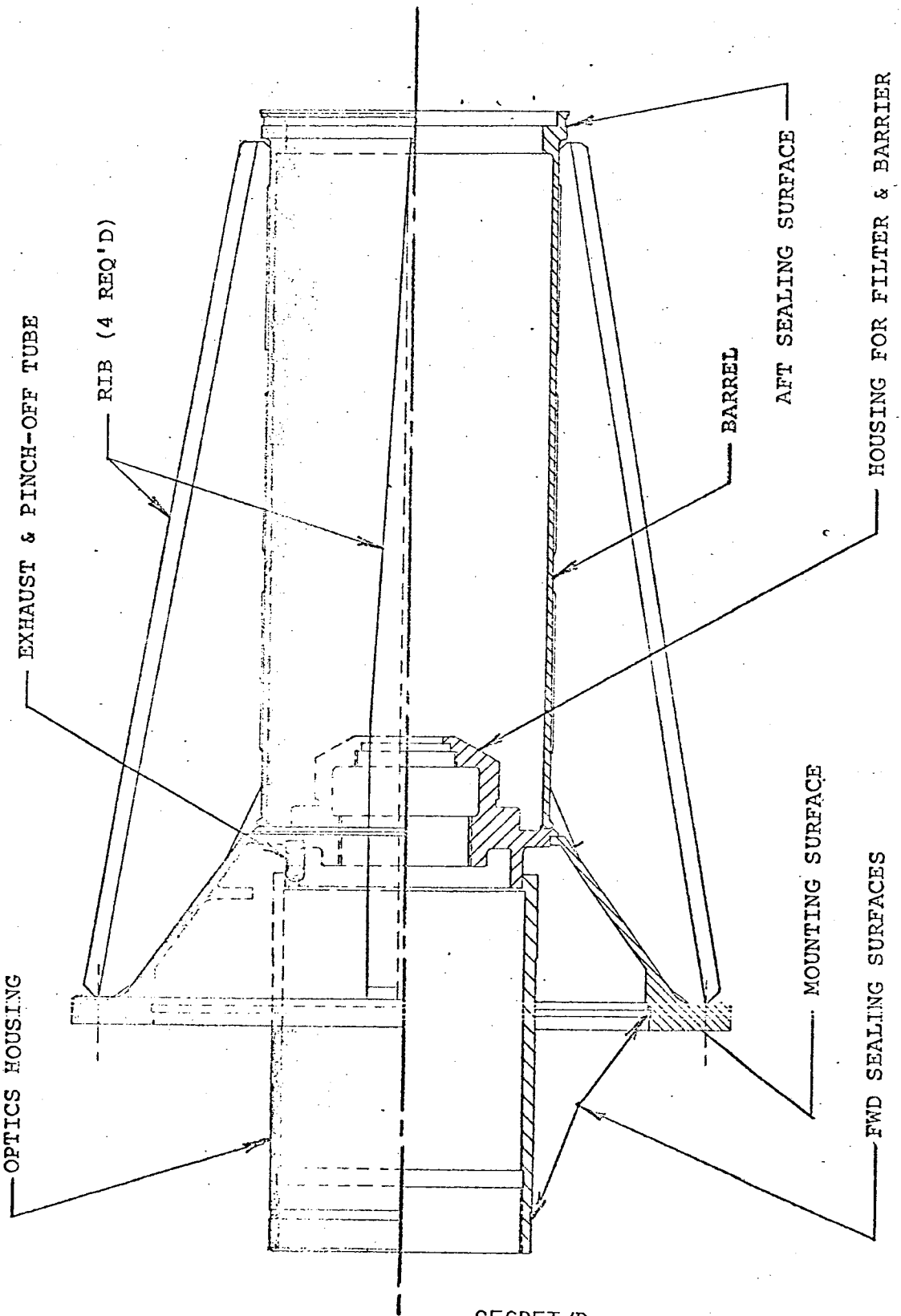

Figure 2.2.1-5. Sensor Body Weldment

Optics

The optics are adjusted for optimum focus and position using a Bench Tester and Alignment Fixture. Measurements are made for each set of optics and then these optics are installed in the sensor using the measurements. Since the alignment fixture duplicates the dimensions of the sensor, the compensation for any tolerance build-up is automatic.

2.2.2 ELECTRONICS ASSEMBLY

The electronics assembly, shown in Figures 2.2.2-1 and 2.2.2-2, is contained in an aluminum case whose outside dimensions are 6.00 x 5.25 x 6.75 inches excluding the mounting flange. Base dimensions including the mounting flange are 6.00 x 6.75 inches.

Outside surfaces of the aluminum case are burnished to a No. 16 finish and given a clear chemical film protective coating. Hemispherical emissivity is $\leq$.15. The total weight of the assembly is 7.90 pounds. Six mounting screw holes are provided in the base mounting flange.

The outer aluminum case has two hermetic (solder) seals; one at the junction of the power supply section with the main body, and a separate seal at the connector or wiring header of the main body. An evacuator-filler tube installed in the power supply section serves both areas in that the RFI seal between the two areas will allow air passage between.

All incoming and outgoing conductor connections are made through a total of three hermetic connectors as follows:

Connector No.	Number of Pins and Wire Size	Function
A2J1	55 - #20	Input and Output Signal Leads
A2J2	32 - #20	Interconnecting Cable to Sensor
A2J3	5 - #16	Power Leads

Wire-wrap pins built into the multi-layer boards provide the terminating method for all internal connections. Power and ground buses also have wire-wrap pins for interconnections.

Electronic circuitry contained within the Electronics Assembly is divided into two main areas. One area consists of the low voltage power supply, and the second area consists of four multi-

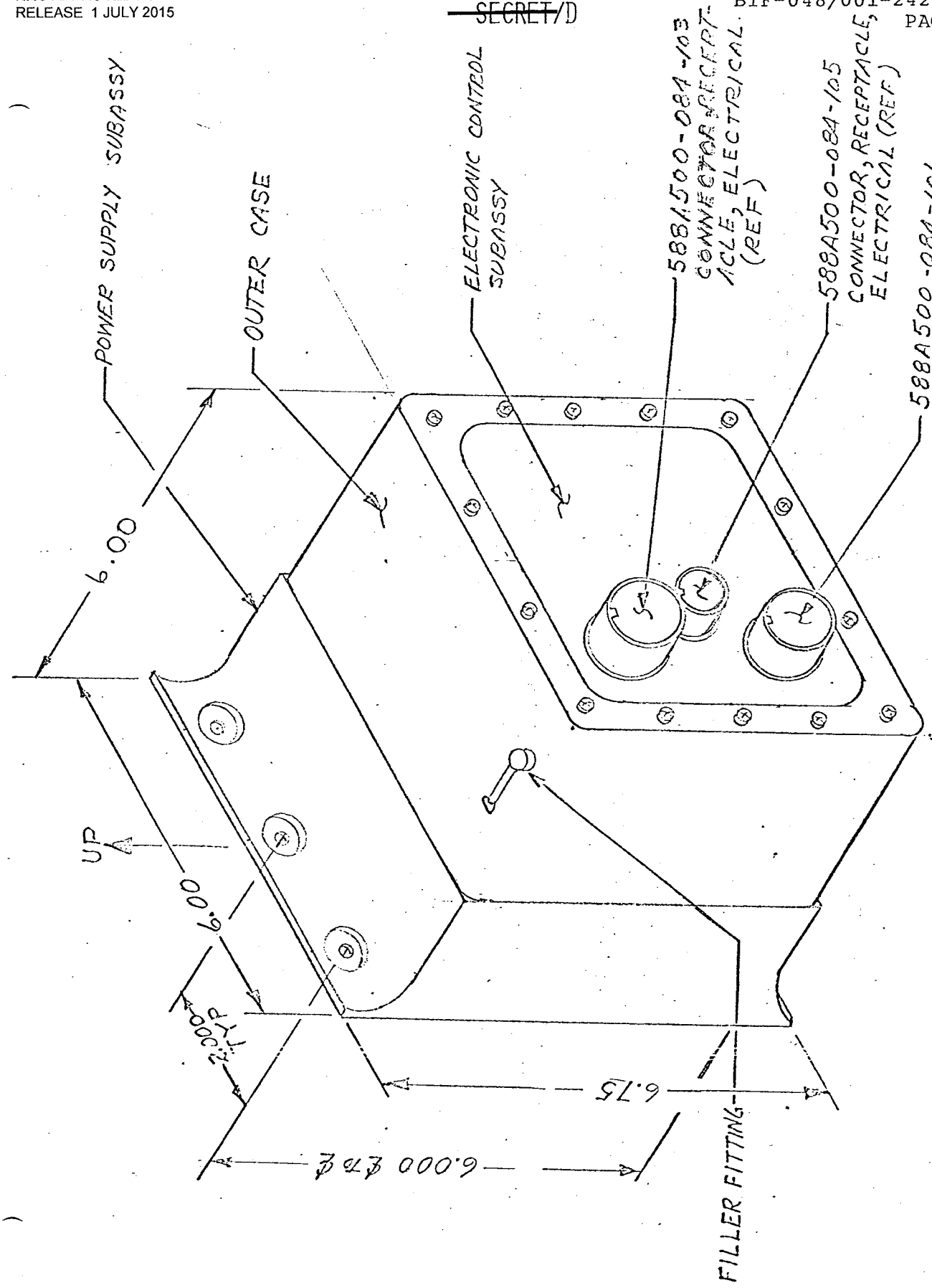

Figure 2.2.2-1. ELECTRONIC CONTROL ASSEMBLY

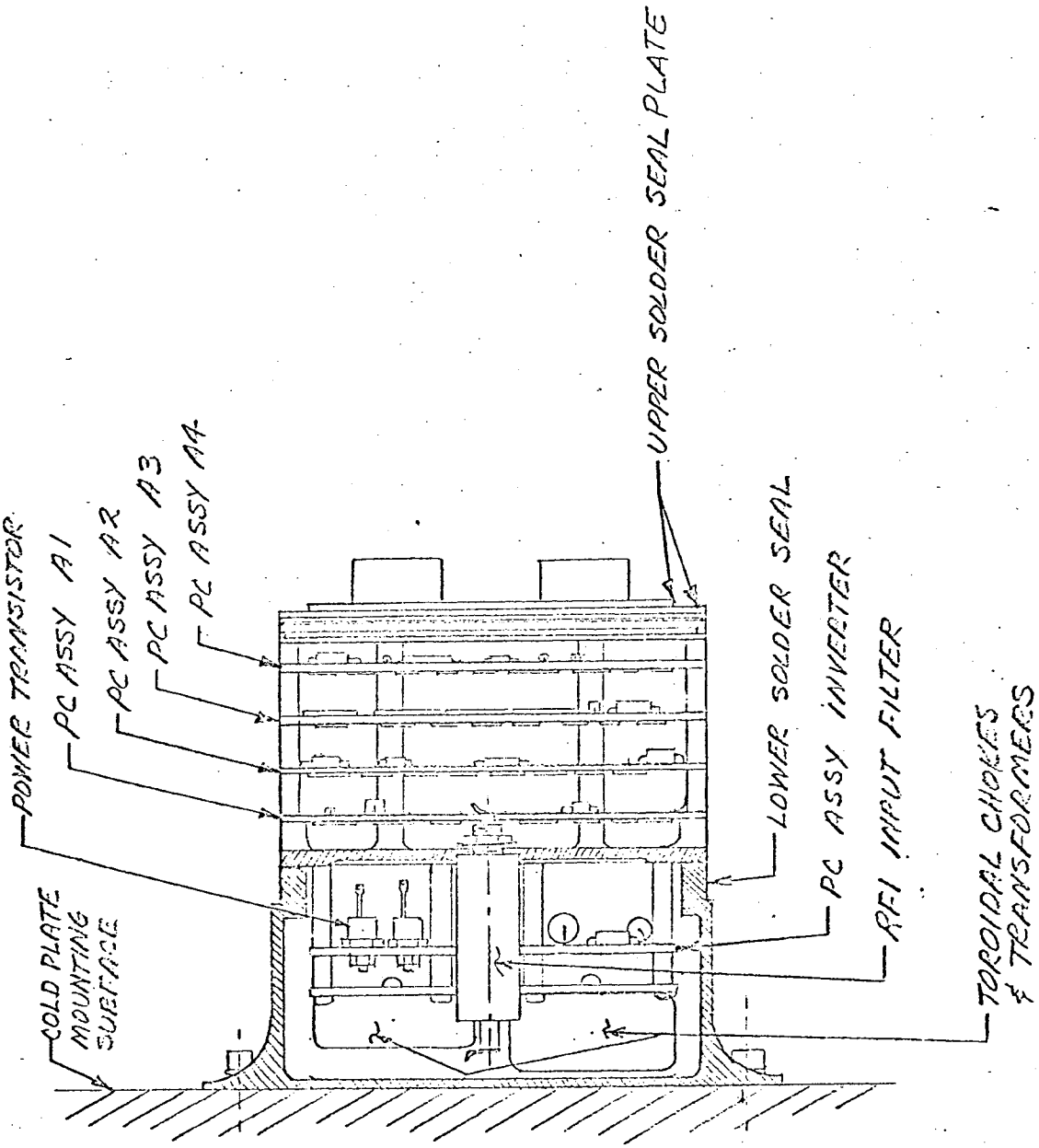

Figure 2.2.2-2.

ELECTRONIC CONTROL SUBASSY

layer printed circuit assemblies of the same size and shape stacked together.

The low voltage power supply (A2A1) is contained in a separate RFI proof compartment within the overall assembly. The low voltage power supply is further divided into three separately shielded sub-assemblies.

The four multi-layer printed circuit assemblies are identified as follows:

Module A2A2	-	Signal Conditioner Assembly
Module A2A3	-	Input-Output Interface Assembly
Module A2A4	-	Control Circuits Assembly
Module A2A5	-	Logic Circuits Assembly

Each of the four assemblies makes use of a maximum amount of integrated circuits and flat-pack, modularized components as compared to discrete components. Wherever possible, the discrete components used have ribbon leads to facilitate the use of reflow solder or welded junctions. Each of the four assemblies has five conductive layers; two power planes (+12V and -12V), two signal planes, and one ground plane.

Some supplementary circuitry associated with, and attached to, each board was added during final checkout. These are in the form of smaller two-sided printed circuits mounted "piggy-back" to the board.

2.2.3 SENSOR ELECTRONICS

Electronic components directly associated with the sensor tube are packaged within the sensor assembly in two areas as follows. Six modules of approximately equal size and shape, but with different circuitry, are installed in the forward section of the sensor package in a close-fitting hexagonal pattern around the optics housing. Two additional electronic assemblies in the form of circular terminal boards with open centers are installed at the rear of the sensor package around the tube base. In addition to serving as interconnecting terminating points for the tube pig-tails, these terminal boards also provide mounting for select-at-test components. These assemblies are identified as A1 and A8.

The six-module grouping in the forward section is surrounded by a ring of wire-wrap terminals to which all wiring from the aft section, plus all wires from the hermetic connector, are permanently terminated. These pins then provide interconnecting terminating points for the module wiring, and for easy replacement of modules without disturbing the permanent sensor wiring.

A description of the six modules follows and the module locations are shown in Figure 2.2.3-1.

Module A2 - High voltage components. Total, 19 components.

Module A3 - Focus control circuit, and erase light control circuit. Total, 20 components.

Model A4 - X and Y deflection control circuits. Total, 19 components.

Model A5 - High voltage control circuit. Total, 40 components.

Model A6 - Filter circuit for 2 KV supply. Total, 8 components.

Model A7 - 2 KV chopper and rectifier circuit. Total, 15 components.

Figure 2.2.3-1.
SENSOR ELECTRONICS

The component count per module is low enough to allow module replacement instead of repair. Components within the modules are mounted either on two-sided P.C. boards, or on multi-layer P.C. boards. These boards, in turn, are epoxied to aluminum plates which serve as heat sinks as well as mounting plates.

A6 and A7 modules are potted with filled epoxy, each being potted in the same size and shape mold.

Conductors from internal circuitry of each module terminate on wire-wrap pins molded in the module and extend out of the module near the wire-wrap pins of the outer terminal ring.

2.2.4 POWER SUPPLY

2.2.4.1 PHYSICAL DESCRIPTION

The Engineering Prototype Evaluation Model DC to DC converter is contained in the bottom 2.75 inch section of the electronics assembly package. The base section also serves as the power supply case. Figure 2.2.4-1 shows the base and the converter assembly. The base weighs 1.8 pounds and the converter assembly weighs 2.9 pounds. The converter is divided into three sections: (1) pre-regulator, (2) oscillator, and (3) series regulator section. A metal divider is placed between the three sections to provide isolation against radiated noise. Isolation between the pre-regulator and the oscillator sections is maintained by using feed-thru ceramic capacitors for the interconnections. The input power passes through an RFI filter section and the operate command line passes through a feed-thru ceramic capacitor. The voltage output terminals from the series regulator section are feed-thru terminals with discrete ceramic capacitors connected between each pin and case ground.

2.2.4.2 THEORY OF OPERATION

A block diagram of the converter system appears in Figure 2.2.4-2. This system utilizes a high efficiency switching regulator as a pre-regulator to provide a nearly constant output voltage over the entire input voltage range of 20 to 33V DC. The pre-regulator also contains the command "ON-OFF" control (operate command) for the entire system. The pre-regulator DC reference voltage is obtained from an auxiliary winding on the low voltage oscillator. This technique makes the pre-regulator compensate for the effects of oscillator transformer loading. In addition, some regulation for the oscillator output sections which are not series regulated is provided. This approach also increases the overall efficiency by allowing the series regulators to operate with a smaller voltage drop across them. The pre-regulator utilizes a flat-pack operational amplifier as a comparator. Three flat-pack dual transistor NPN-PNP units are used for signal conditioning and control. The final three stages of switching transistors are discrete units with the final transistor capable of switching 10 amperes. This unit uses the switching

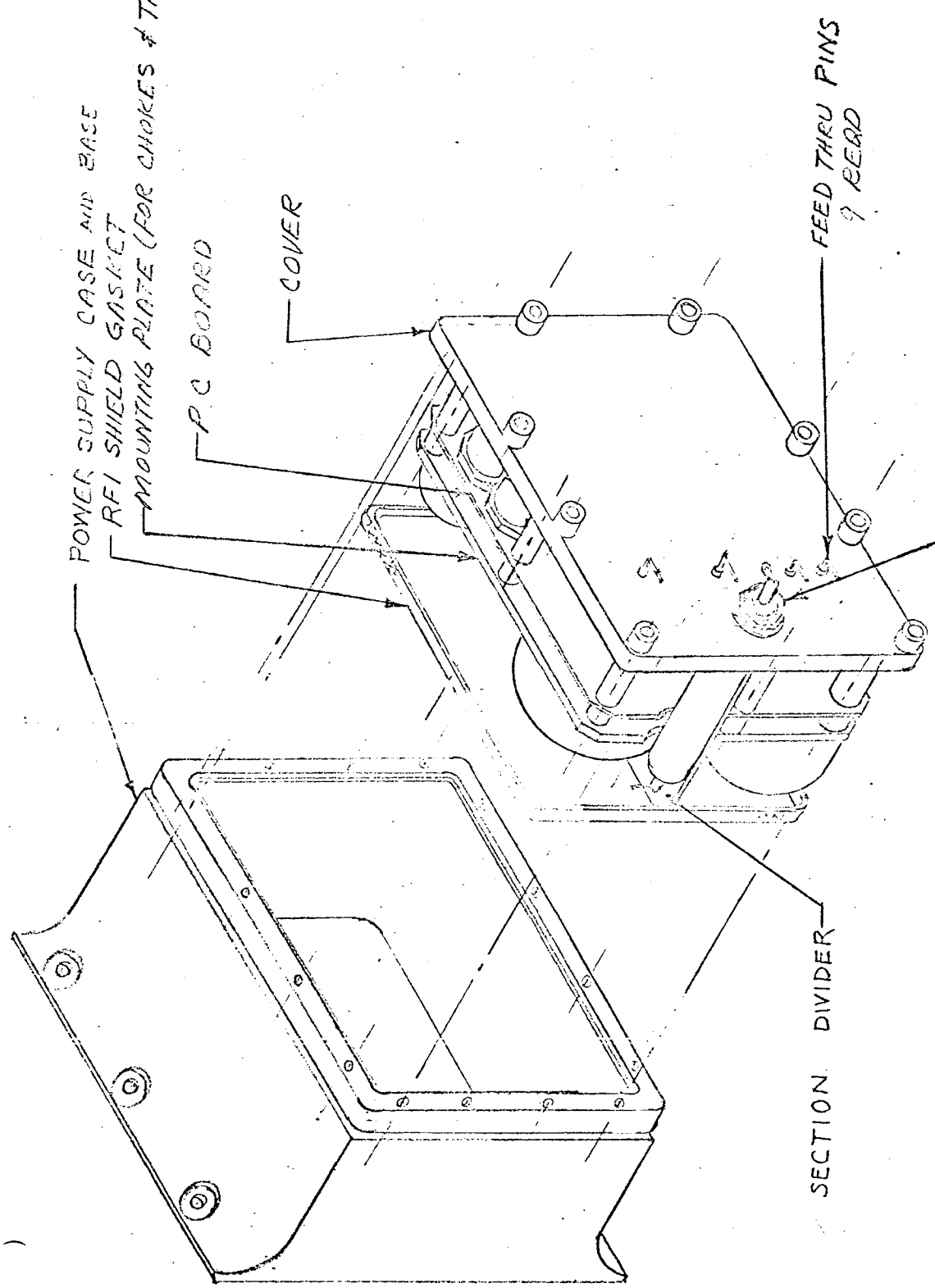

Figure 2.2.4-1. Low Voltage Converter and Case

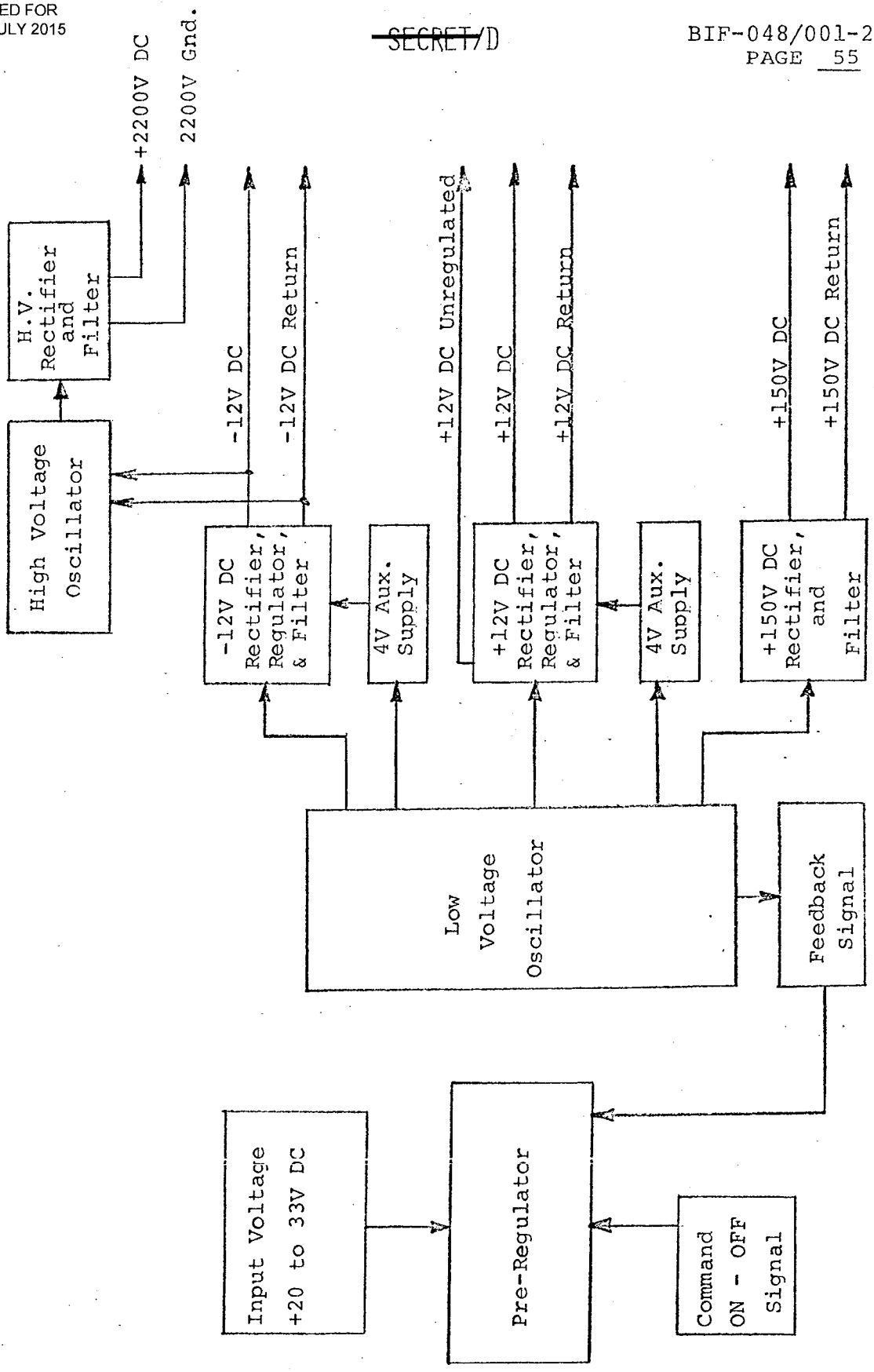

Figure 2.2.4-2. DC to DC Converter Block Diagram

inductor as a current transformer to generate an additional voltage to the four stages preceding the switching transistor. Thus the pre-drivers drive the switching transistor into saturation and consequently reduce the power loss in the switching transistor.

The low voltage oscillator is a dual-transformer type. The dual-transformer oscillator depends on a small saturating tape-wound toroidal transformer for switching while a larger nonsaturating power transformer generates the feedback and output power transformation. This approach reduces the switching transients associated with the conventional single saturating transformer and helps improve the oscillator efficiency. The power transformer provides outputs for the +150V DC, $\pm$12V DC, a feedback winding, and two auxiliary sources. The auxiliary windings are used to increase the efficiency of the plus and minus 12 volt series regulator sections.

The series regulator section contains the required rectifiers, regulators, and filters. The 150V DC section has a full-wave bridge rectifier and a single L-C filter section. The plus and minus 12V DC sections contain discrete component full-wave rectifiers, miniature integrated circuit DC voltage regulators driving discrete high current transistors, and capacitive filters. The two regulated outputs are short circuit proof. They have a fold-back current limiting feature to reduce the power dissipation of the series regulators in the event of a short circuit. The plus 12V DC unregulated output is taken from the plus 12V DC regulated section before it is series regulated. The term "unregulated" output refers to regulation better than 0.15% for a 10% load variation without the series regulators. This regulation is a result of the oscillator feedback to the pre-regulator. Two auxiliary supplies are used to increase the voltage on the integrated circuit regulators and, in turn, reduce the power loss through the high current series regulators.

The high voltage oscillator is also a dual-transformer type. The output of the oscillator feeds a full-wave bridge rectifier and a voltage doubling circuit. The output of the voltage doubling circuit feeds two L-C filters and one R-C section. The input to

the high voltage oscillator is taken from the minus 12 volt regulated output. This source serves two purposes: It (1) provides a stable low impedance source for the high voltage section, and (2) a current limited input to the high voltage unit. The current limited input provides indirect short circuit protection for the high voltage supply.

The overall supply efficiency has been measured at 65% over the full line voltage input range of 20 to 33 volts.

2.3 EPEM ACCEPTANCE TEST RESULTS AND COMPARISON WITH PERFORMANCE REQUIREMENTS

Acceptance testing was performed on the EPEM in accordance with PAUL Final Acceptance Test Procedure (see Ref. 4). The acceptance test results are compared with EC-701A Rev. 5 requirements in this section and a summary of the comparative results are summarized in section 1.3 (EPEM Performance Status) of this report.

Optical focus variation and cloud obscuration tests, along with portions of other tests, were not performed in order to meet the EPEM delivery schedule. In addition, it was planned to perform the acceptance tests using both PAUL #1 and #8 scenes and M&M scenes. The M&M scenes were acquired too late to be used in the acceptance testing.

The test results shown in this section are summarized for clarity of comparison and interpretation and will not, in all instances, exactly follow the test result format for reduced data given in the Acceptance Test Results section of Ref. 4.

2.3.1 INITIAL CONDITION TESTS

The initial condition tests were conducted using the PAUL #1 scene. The specification requirement applying to this test is the maximum two minute warm-up time requirement. The complete EPEM warm-up required 13.72 seconds which is well within the required warm-up time.

2.3.2 DYNAMIC RANGE AND LINEARITY

A plot of X and Y indicated vs. true image velocity in the large signal region is shown in Figure 2.3.2-1. As can be seen from the plot, the EPEM indicated vs. true image velocities fall within the indicated specification requirements of EC-701A Rev. 5.

Also during this test, it was found that left rate motion at the subsystem optical interface produced a rate polarity indication of zero volts and right rate motion caused a sense voltage of 4.5V DC (logical one) for rate polarity indications which complies with the specification requirement.

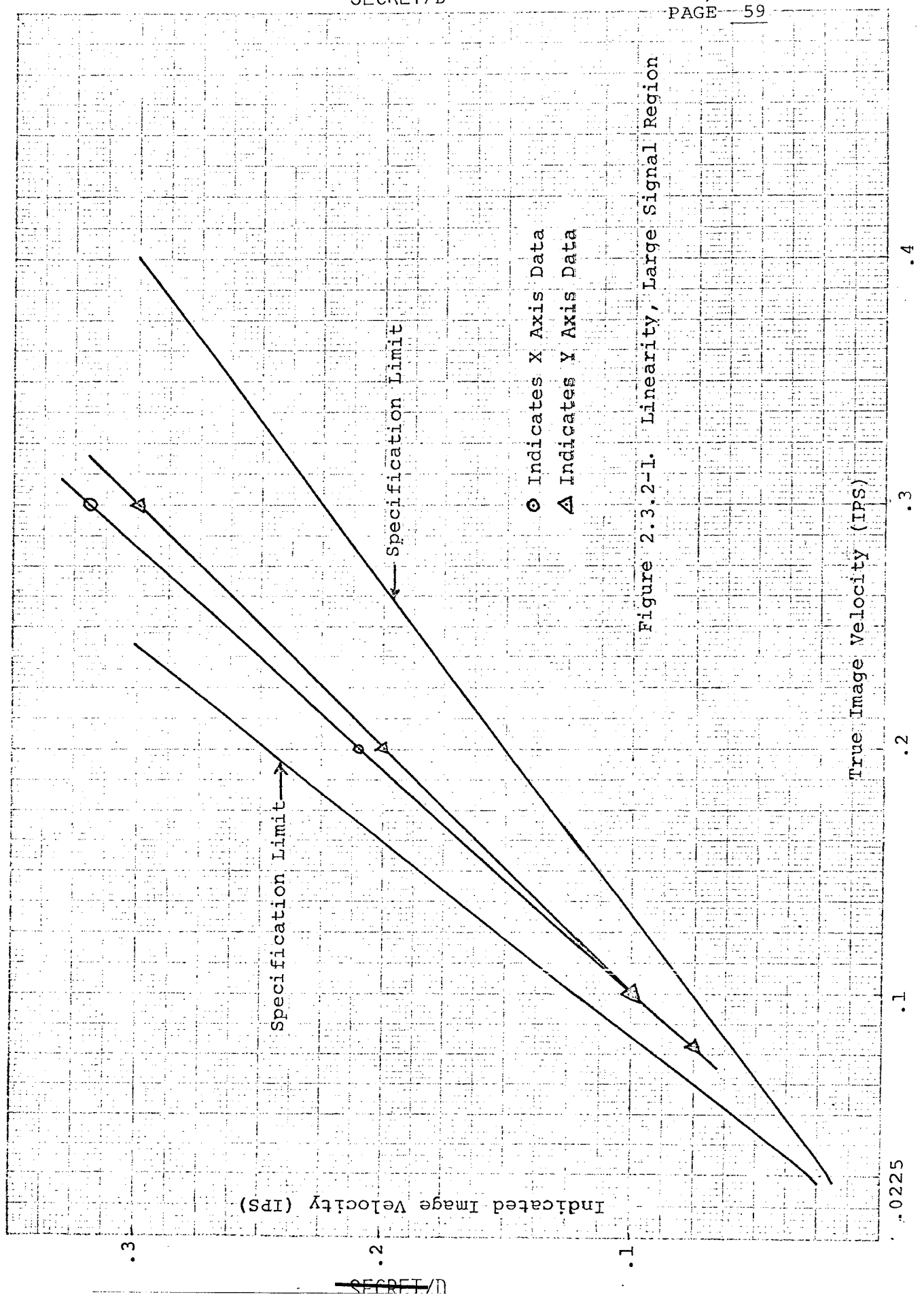

Figure 2.3.2-1. Linearity, Large Signal Region

2.3.3 SATURATION INDICATION

The rate saturation outputs met the specification requirements for positive rate saturation signals at 0.3 IPS and negative rate saturation signals at 0.31 IPS.

2.3.4 NOISE AND BIAS

The null accuracy evaluation tests were conducted utilizing three channels of analog information. The X and Y rate outputs and a 2.5V DC reference was transmitted over Bell Telephone Lines to an analog to digital converter and the digital information stored on magnetic tape. The noise and bias data was then evaluated using an IBM 360 programmed for the mathematical sequence outlined in Figure 2.3.4-1. Terminology definitions are given in Figure 2.3.4-2. All Power Spectral Density Data was obtained using a Fast Fourier Transform technique.

Tests IV A and B were conducted and the resultant data is indicated in Table 2.3.4-1. Tests A and B were run for one high light level and one low light level. Since available time was critical and the tests were considered representative, the remaining tests were not conducted.

There are three stages necessary in the processing of random noise data for compliance to para. 3.1.1.1.1.C of EC-701A Rev. 5. These include determining the power spectral densities at the output of the BETA Subsystem and the output of the sampler along with the PSD obtained after application of an attenuation factor to the sampler output. A block diagram showing these three stages can be seen in Figure 2.3.4-3. Also noted in the same figure are the locations of PSD plots obtained for Acceptance Test IV A and IV B.

In reviewing the PSD data, a very large amount of energy was found to be concentrated at 57 hertz. The amount of energy contained in the 57 Hz region was the major contributor to the total periodic noise figure and it was found that this frequency could be filtered out with a notch filter at the rate outputs. However, the PSD results shown in this report were derived from unfiltered rate outputs.

MATHEMATICAL SEQUENCE TO DETERMINE THE TOTAL CONTRIBUTION OF NOISE AND BIAS

BIAS

B_x & B_y

$$B_T = \sqrt{B_x^2 + B_y^2}$$

PERIODIC NOISE

Primary Periodic Noise

A_{i_x}, A_{i_y}

K_{i_x} & K_{i_y}

Complementary Periodic Noise

$A_{i_{cx}}$, $A_{i_{cy}}$

$K_{i_{cx}}$ & $K_{i_{cy}}$

$$N_{xp} = \sum^{i} K_{i_x} A_{i_x} + \sum^{i} K_{i_{cx}} A_{i_{cx}}$$

$$N_{yp} = \sum^{i} K_{i_y} A_{i_y} + \sum^{i} K_{i_{cy}} A_{i_{cy}}$$

RANDOM NOISE

Φ_x^*, Φ_y^* & Appropriate Attenuation Characteristics of Fig. 5A or 5B (Abbr. of Last Parts A.A.C.)

$$\Phi_{ccx} = (\Phi_x^*) \text{ (A.A.C.)}$$

$$\Phi_{ccy} = (\Phi_y^*) \text{ (A.A.C.)}$$

$$N_{xr} = 2\sqrt{\frac{1}{\pi}\int_0^{\infty} \Phi_{ccx}\, d\omega}$$

$$N_{yr} = 2\sqrt{\frac{1}{\pi}\int_0^{\infty} \Phi_{ccy}\, d\omega}$$

$$N_x = N_{xp} + N_{xr}$$

$$N_y = N_{yp} + N_{yr}$$

$$N_T = \sqrt{N_x^2 + N_y^2}$$

Total Combination of Noise and Bias = $N_T + B_T$

Figure 2.3.4-1.

SECRET/D

SECRET/D

A = Half amplitude of each periodic frequency - IPS

$A_{i_{cx}}$ = Half amplitude of the complementary periodic frequencies about the X axis - IPS

$A_{i_{cy}}$ = Half amplitude of the complementary periodic frequencies about the Y axis - IPS

A_{i_x} = Half amplitude of the primary periodic frequencies about the X axis - IPS

A_{i_y} = Half amplitude of the primary periodic frequencies about the Y axis - IPS

B_T = Total bias - IPS

B_x = Bias of the X axis - IPS

B_y = Bias of the Y axis - IPS

$K_{i_{cx}}$ = Attenuation factor for the half amplitude of the complementary periodic frequencies about the X axis - db

$K_{i_{cy}}$ = Attenuation factor for the half amplitude of the complementary periodic frequencies about the Y axis - db

K_{i_x} = Attenuation factor for the half amplitude of the primary periodic frequencies about the X axis - db

K_{i_y} = Attenuation factor for the half amplitude of the primary periodic frequencies about the Y axis - db

N_T = Total noise - IPS

N_x = Sum of random component and total periodic noise about the X axis - IPS

N_{xp} = Total periodic noise about the X axis - IPS

N_{xr} = Random component of noise about the X axis - IPS

N_y = Sum of random component and total periodic noise about the Y axis - IPS

N_{yp} = Total periodic noise about the Y axis - IPS

N_{yr} = Random component of noise about the Y axis - IPS

Figure 2.3.4-2. Noise & Bias Terminology Definitions (Sheet 1)

Φ_{ccx} = Resultant PSD about the X axis - IPS^2/Hz (Found by mult. Φ_x^* by the appropriate attenuation characteristic)

Φ_{ccy} = Resultant PSD about the Y axis - IPS^2/Hz (Found by mult. Φ_y^* by the appropriate attenuation characteristic)

Φ_x^* = Sampled PSD about the X axis - IPS^2/Hz

Φ_y^* = Sampled PSD about the Y axis - IPS^2/Hz

Figure 2.3.4-2. Noise & Bias Terminology Definitions (Sheet 2)

TABLE 2.3.4-1. NOISE AND BIAS ERROR RESULTS

	Test No. IV-A PAUL #1 0.05 μa Illum. Level	Test No. IV-B PAUL #1 0.40 μa Illum. Level
X-Bias	0.0005 IPS	0.0005 IPS
X-Periodic Noise	0.0124 "	0.0067 "
X-Random Noise	0.0200 "	0.0087 "
X-Total Noise	0.0324 "	0.0154 "
Y-Bias	0.0009 "	0.0009 "
Y-Periodic Noise	0.0098 "	0.0032 "
Y-Random Noise	0.0106 "	0.0045 "
Y-Total Noise	0.0204 "	0.0078 "
Total Bias	0.0011 "	0.0010 "
Total Noise	0.0383 "	0.0173 "
Total Bias and Noise	0.0394 "	0.0183 "

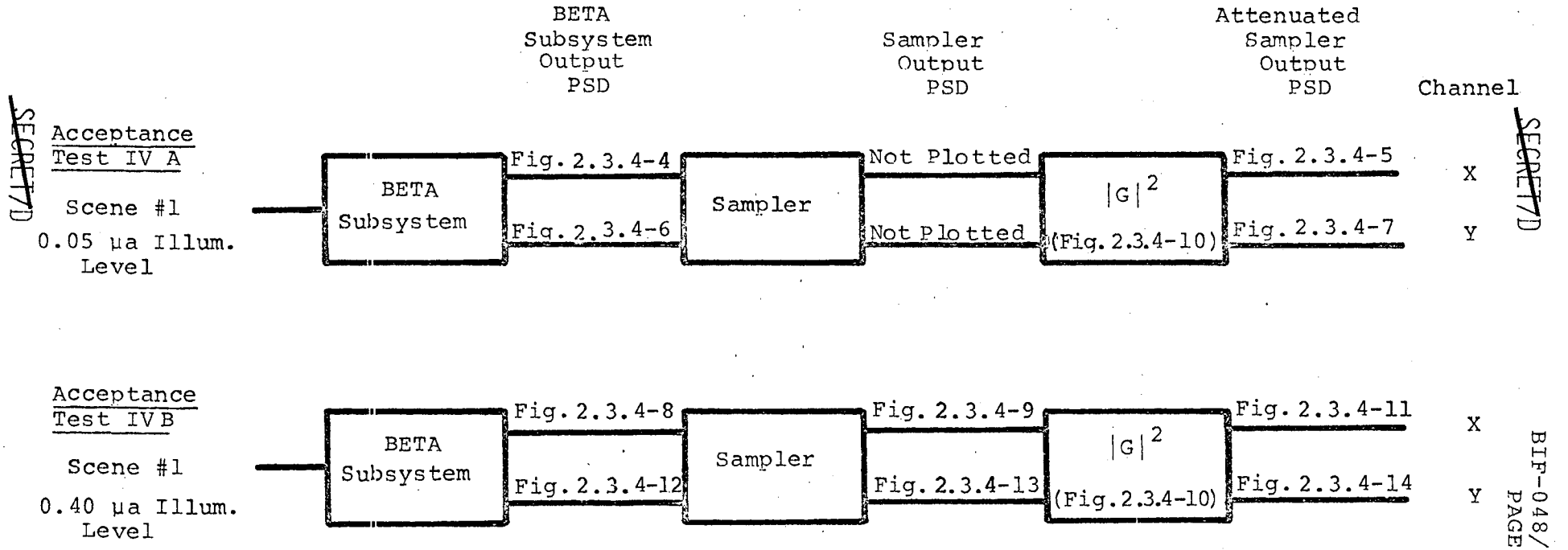

Figure 2.3.4-3. Noise PSD Plot Summary

The value of the bias term appears to have some error due to the 2.5V DC reference level. The bias level is obtained by using all the data up to one hertz. This data is first processed by subtracting 2.5V DC assuming there is no line loss in transmission and that the single ground reference transmitted has the same potential as the rate output references. In reality, there is probably a sufficient amount of error involved in these assumptions which would contribute toward making the bias term larger than it should be.

In spite of the probable errors in the data, there still is a random noise problem which will have to be investigated. At this time, the EPEM does not comply with EC-701A Rev. 5 requirements for null accuracy. The value of total bias and noise obtained from the final acceptance test data has a value of 0.0394 IPS for the low illumination scene and 0.0183 IPS for a high illumination scene compared to the specification allowable level of 0.01 IPS. Methods for reducing the system levels are discussed in section 1.4.1.4 of this report.

Considerable reduction in periodic noise could be achieved if the amplitude of each periodic sinusoid was multiplied by the change in cumulative power as required by the latest revision of the specification EC-701B paragraph 3.1.1.1.1.C. (see Ref. 5).

2.3.5 THRESHOLD AND NULL LINEARITY

Only one section of this test was performed due to the limited amount of time available and the amount of time necessary in reducing and analyzing the data from small signal low light level data. The data taken was obtained with an illumination level of 0.4 μa of cathode monitor current. The data is shown in Table 2.3.5-1.

The data is plotted in Figure 2.3.5-1. The boundary conditions for this curve were taken from Figure 2 of specification EC-701A Rev. 5. The indicated vs. true velocities for both axes can be seen to be within the allowable specification requirements.

Fig. 2.3.4-4. Acceptance Test Procedure Test IV A - BETA Subsystem Channel X Output PSD

Fig. 2.3.4-5. Acceptance Test Procedure Test IV A -
Channel X Attenuated Sampler Output PSD

Fig. 2.3.4-6. Acceptance Test Procedure Test IV A - BETA Subsystem Channel Y Output PSD

Fig.2.3.4-7. Acceptance Test Procedure Test IV A - Channel Y Attenuated Sampler Output PSD

Fig.2.3.4-8. Acceptance Test Procedure Test IV B - BETA Subsystem Channel X Output PSD

Fig.2.3.4-9. Acceptance Test Procedure Test IV B - Channel X Sampler Output PSD

Fig.2.3.4-10. Attenuation Factor for Sampler PSD

Fig. 2.3.4-11. Acceptance Test Procedure Test IV B -
Channel X Attenuated Sampler Output PSD

Periodic

Fig. 2.3.4-12. Acceptance Test Procedure Test IV B - BETA Subsystem Channel Y Output PSD

Fig. 2.3.4-13. Acceptance Test Procedure Test IV B -
Channel Y Sampler Output PSD

Fig.2.3.4-14. Acceptance Test Procedure Test IV B -
Channel Y Attenuated Sampler Output PSD

TABLE 2.3.5-1 - THRESHOLD AND NULL LINEARITY DATA

P/P POSITION (Inches)	INPUT PEAK X OR Y RATES (IPS)	MEASURED PEAK RATES (IPS)	
		X	Y
.004	.00247	.0025	.0025
.0063	.00389	.0035	.0035
.0084	.00519	.0045	.0050
.01075	.00663	.0060	.0065
.0122	.00753	.0065	.0075
.01385	.00855	.0075	.0085
.0168	.01038	.0085	.0100
.0186	.01148	.0095	.0110
.0200	.01235	.0105	.0120

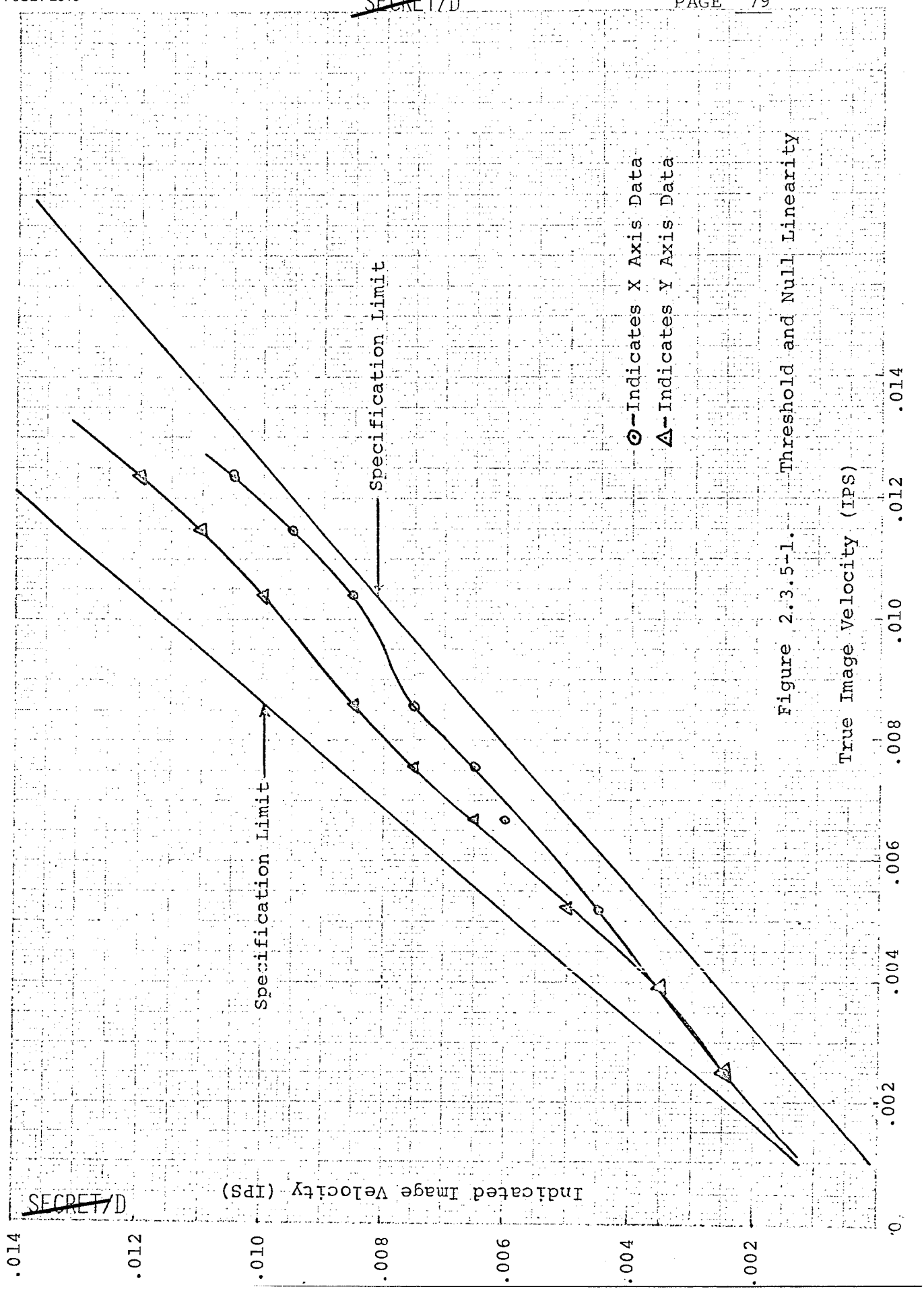

Figure 2.3.5-1. Threshold and Null Linearity

2.3.6 FREQUENCY RESPONSE

Data for the frequency response was taken on the PAUL #1 scene at a cathode current of 0.4 μa to expedite testing and data reduction. This data will be representative for all conditions of subsystem frequency response with the possible exception of variations occurring in interpretation of data. Low density scenes with low light levels necessarily produce more noise in the indicated rate data and increase the difficulty in obtaining phase and gain information.

The data from the X channel was plotted on Figure 2.3.6-1 and both phase and gain indicate a single lag at approximately 3.5 Hz. Gain and phase measurements are within the EC-701A Rev. 5 requirements for a single lag to a frequency of 15 Hz which was the maximum frequency limitation of the test equipment used. Previous information dealing with theoretical system response (Ref. 6) indicates that deviations in gain and phase greater than the required limits can be expected at frequencies greater than 100 Hz.

The BETA Subsystem frequency response is related to the output PSD requirement, however. Each of these requirements can be satisfied independently. Trade-offs between these two areas will be required in order to obtain satisfactory system performance.

2.3.7 EFFECTS OF ILLUMINATION AND CONTRAST

Tests on the PAUL #1 scene indicated the CCU light could be increased until the total light level was 8.6 times the original scene light for satisfactory system operation. PAUL #1 scene has an average contrast of 33.3% and the addition of CCU dropped the contrast to 3.9%. Tests on the PAUL #8 scene, with an original contrast of 13%, would allow the system to operate with CCU added which dropped the contrast to 7.2%. The difference in minimum operating contrast between the two scenes is due to the frequency content of the different scenes with PAUL #1 scene representing a low spatial frequency condition and scene #8 a high frequency scene.

Figure 2.3.7-1 is a plot of one-dimensional Wiener Spectrum content expressed in db versus image plane average light level expressed in footcandles. The data is identified and indicates constant contrast lines for PAUL #1 and #8 scenes. The line

SECRET/D

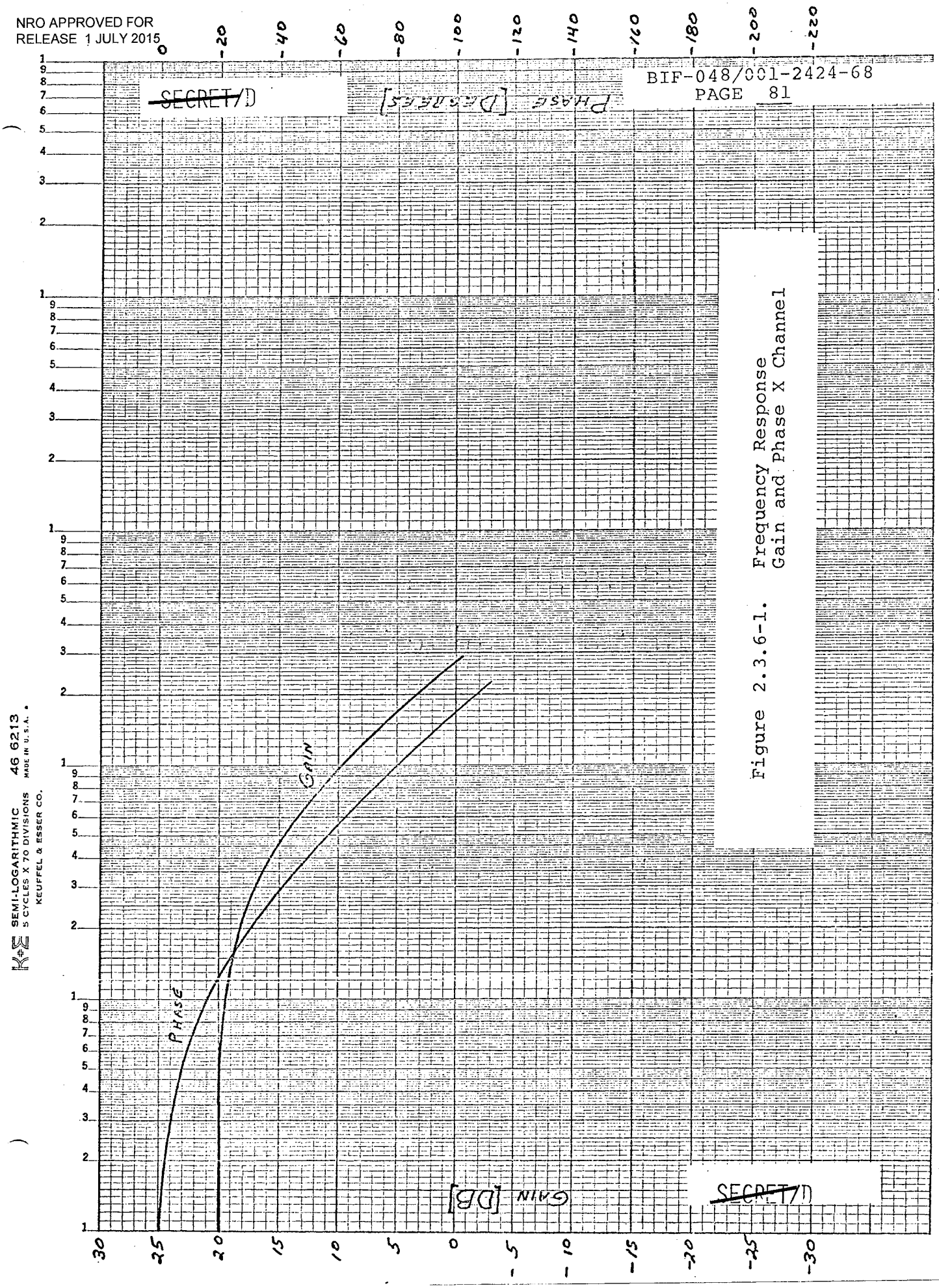

Figure 2.3.6-1. Frequency Response
Gain and Phase X Channel

SECRET/D

SECRET/D

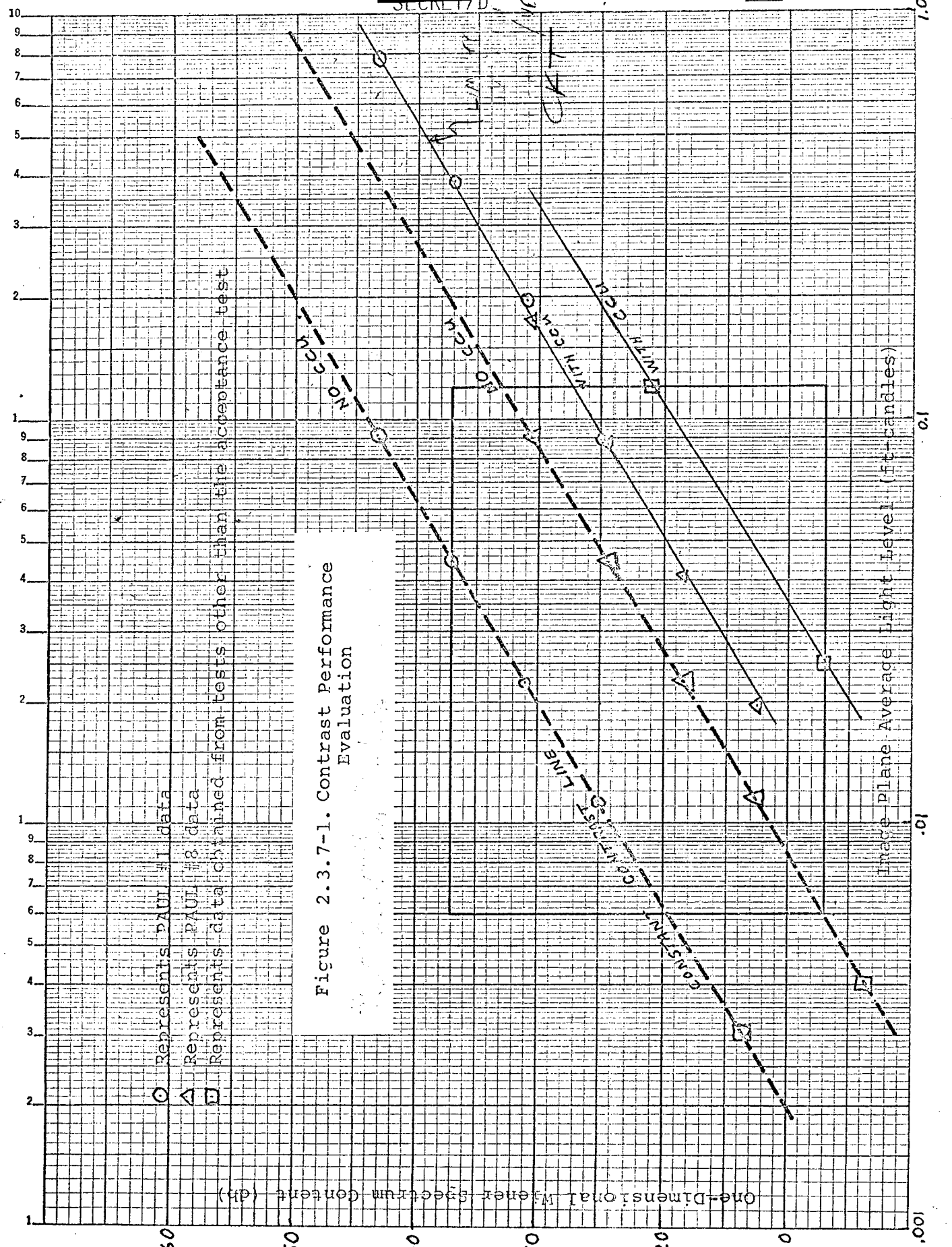

Figure 2.3.7-1. Contrast Performance Evaluation

SECRET/D

representing both PAUL #1 and #8 is the present operation of the EPEM unit with the addition of CCU. The remaining line represents data obtained from previous tests performed before the final acceptance test. The apparent difference between the two curves was due to increased noise and the effect of the noise on the present track verify settings. The enclosed rectangle represents the area of interest for operation based on specification EC-701A, Rev. 5.

A discussion of methods which can be used to improve low contrast performance is given in section 1.4.1 of this report.

2.3.8 VOLTAGE VARIATIONS

The voltage variation tests were conducted according to the input levels outlined in the final acceptance test procedure. The procedure calls for operation by varying the system input power from 20 to 33V DC which includes the abnormal power range of the specification. The system remained operational throughout the entire run; however, the noise on the rate outputs were excessive with a 20V DC input. When the input voltage reached 23V DC the noise suddenly dropped in magnitude. This effect is caused by the internal unregulated supply voltage dropping to the level where the focus control stops regulating. In checking the supply input, it was noted that there was about 1.5V DC dropped in control box and long cables. One reason for the voltage drop is a result of a series diode in the Ancillary Tester Programmer to protect the system against a polarity reversal on the input power.

The BETA Subsystem does not contain protective diodes. Further, the input voltage was measured at the input power supply and before the voltage drop encountered in the Programmer. Therefore, the present system would not be expected to show a rate noise increase at low supply voltages (20-23V DC). Several BETA power supply modifications can be made, if necessary, on the system which will improve the efficiency of the focus control circuitry and thereby allow increased system performance over a wider range of input voltages than the present system will allow.

2.3.9 OPTICAL FOCUS VARIATION

These tests were not conducted during the final acceptance tests due to the required delivery schedule. However, these tests have been performed in the past, and no noticeable effect on system performance using average scenes have been noticed.

2.3.10 CLOUD OBSCURATION

These tests were not conducted since they were not related to a direct specification requirement. The results of cloud obscuration testing using the PAUL breadboard (Ref. 7) and are considered representative of the results which would be expected using the EPEM.

2.3.11 DYNAMIC NULL TESTS

The results of dynamic null tests are summarized in Table 2.3.11-1. It should be noted that values of X and Y velocity are given minus the component due to null noise and, therefore, indicate only those velocities introduced by distortion of the scene and the simulator focal length used. Data with the optical nutator running are given minus the sine wave component due to the nutator.

M&M scenes were not available in time for evaluation. Due to the EPEM delivery schedule not all of the dynamic null tests were run with both PAUL scenes; however, sufficient tests were run which allow adequate evaluation of system performance during dynamic null.

In all cases, the indicated rates were less than 0.01 in/sec. and showed a random distribution as scene, roll angle and light level were varied. An explanation of dynamic null errors for simulator vs. real case geometry is given in section 1.4.1 - Performance Improvements.

Test No.	PAUL Scene No.	Cathode Current μa	Total CCU μa	Roll Angle	Optical Nutator	Average Track Length	Total Track Length	No. of Cycles	X Vel. Ave. IPS	Y Vel. Ave. IPS
10A	1	0.05	No	0°	No	7.7°	66.2°	8	0.0095	0.0044
11A	1	0.05	No	20°	No	6.01°	66.4°	10	0.0055	0.0096
11I	1	0.05	No	40°	No	5.96°	58.7°	9	0.0059	0.0028
12A	1	0.05	0.25	0°	No	3.78°	42.4°	10	0.0059	0.00038
13A	1	0.05	No	0°	Yes	7.04°	61°	8	0.0062	0.0009
10B	1	0.40	No	0°	No	24.9°	74.6°	3	0.0098	0.0060
11B	1	0.40	No	20°	No	33.4°	25.6°	3	0.0042	0.0012
11J	1	0.40	No	40°	No	28.9°	58.5°	2	0.0073	0.0058
12B	1	0.40	2.4	0°	No	4.76°	53.4°	10	0.0075	0
13B	1	0.40	No	0°	Yes	12.9°	66.9°	5	0.0076	0
14A	1	0.05	0.25	0°	Yes	1.35°	18°	10	0	0.013
14B	1	0.40	2.4	0°	Yes	5.62°	60.9°	10	0.0049	0.0019
10D	8	0.40	No	0°	No	4.14°	44.3°	10	0.0039	0.0022
11D	8	0.40	No	20°	No	5.08°	54.7°	10	0.0080	0

TABLE 2.3.11-1 - DYNAMIC NULL TEST SUMMARY

2.4 EPEM IMPROVEMENTS

2.4.1 WEIGHT

The present EPEM weight is 22.7 pounds which is composed of 7.9 pounds for the Electronics Assembly and 14.80 pounds for the Sensor Assembly. The total weight requirement for the BETA Subsystem of 22 pounds was not met. This is due to the sensor package weight of 14 pounds not being met. Several methods of reducing the Sensor Assembly weight are available and will be explained in the following section.

2.4.1.1 SENSOR ASSEMBLY WEIGHT REDUCTION

A stress analysis of the sensor was made (see Ref. 8). The results indicate that the present stiffeners used on the sensor body are not required and could be eliminated resulting in a weight reduction of approximately 0.8 pounds (Ref. 9). Thinner metal could be used in other areas of the sensor housing reducing the weight even further. With these changes the BETA Sensor Assembly weight would be less than the required 14 pounds.

A three pound weight is estimated for the mounting adapter which is required as interface between the BETA Subsystem Sensor Assembly and vehicle mounting surface.

A redesign of the Sensor Assembly can be made in which the mounting adapter could be incorporated with a resultant saving in weight and number of parts required. As shown in Figure 2.4.1-1, this redesign has the additional advantage of allowing the Sensor Assembly center of gravity to be located on-axis and closer to the center of the assembly (4.90 inches from image plane) than presently located. This estimated redesign weight is 14.33 pounds. Excluding the 3 pound allowance for the adapter, the effective Sensor Assembly weight would be 11.33 pounds as shown in Table 2.4.1-1. The redesign would also encompass changes in the coil forms and positioning of the electronic modules.

SECRET/D

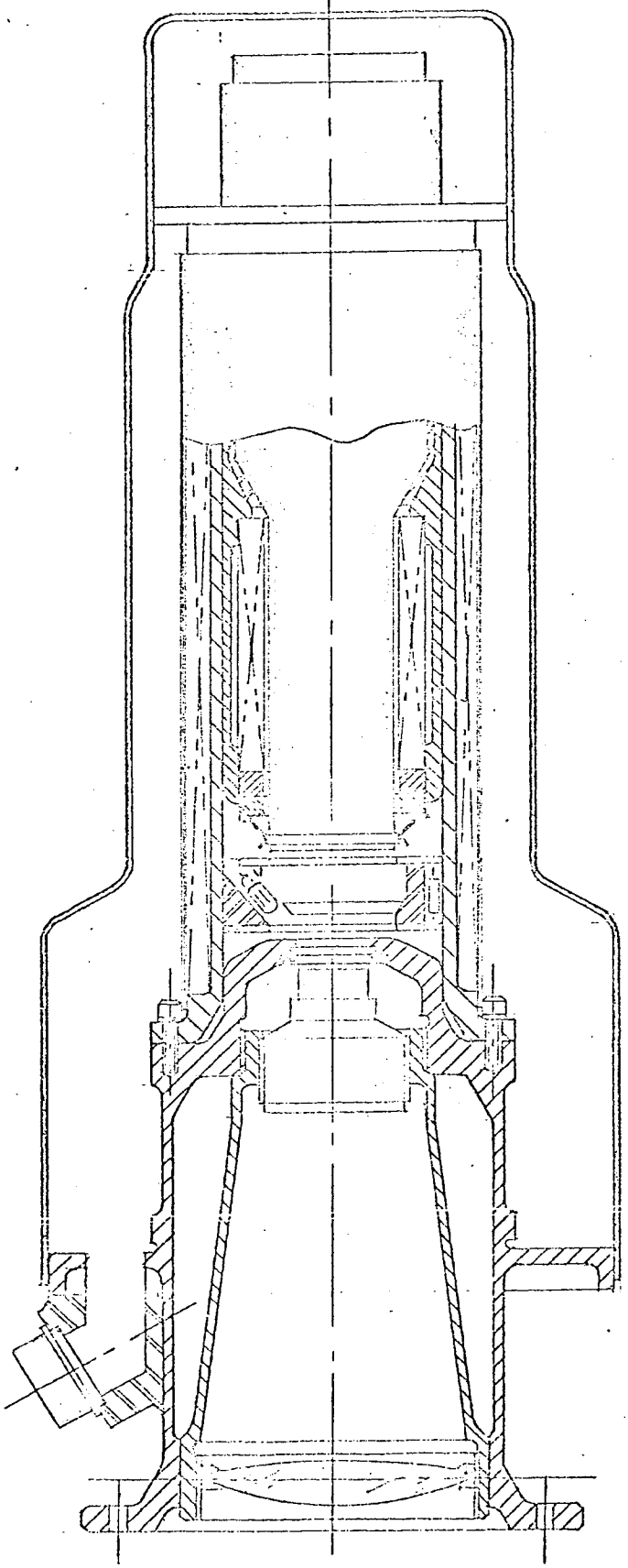

SECRET/D

Figure 2.4.1-1. Proposed Sensor Assembly with Mounting Adapter Included and With a Separate Optical Subassembly

TABLE 2.4.1-1 - SENSOR WEIGHT ESTIMATE

FIELD LENS ASSEMBLY	0.32
FIELD LENS LOCK RING	0.03
BARRIER	0.02
BARRIER LOCK RING	0.03
RELAY LENS LOCK RING	0.02
RELAY LENS ASSEMBLY	0.23
ERASE LIGHT ASSEMBLY	0.28
SHIELD	0.65
CONTACT RING ASSEMBLY	0.06
CONNECTOR	0.05
EXHAUST TUBE	0.03
DEFLECTION COIL	0.56
MAIN SUPPORT HOUSING	2.52
OPTICS HOUSING	0.77
FOCUS & DEFLECTION COIL ASSEMBLY	6.07
TUBE ASSEMBLY	0.89
COVER & SOLDER	1.00
ELECTRONICS & WIRE	0.80
ESTIMATED WEIGHT	14.33
ADAPTER WEIGHT	3.0
EFFECTIVE SENSOR WEIGHT	11.33 LBS.

By using the shorter tube discussed in section 3.2.3, the proposed Sensor Assembly could be shortened as shown in Figure 2.4.1-2 and provide an additional saving in weight. The total Sensor Assembly weight would then be an estimated 13.3 pounds. Since this weight includes the incorporation of the required interface mounting, the effective weight of the Sensor Assembly would be 10.3 pounds due to the 3.0 pound allowance for the mounting adapter.

2.4.2 POWER

The EPEM, at present, requires 25 watts average power. This power can be reduced 20 to 30% by changing the present Amelco Logic to the R.C.A. MOS FET logic now available in mil-spec ratings. The R.C.A. MOS FET logic requires only 10 nanowatts of power per gate and has all the advantages of the presently used Amelco HNIL which requires 20 milliwatts per gate.

A further reduction of 4% can be obtained by reducing the length of the drift section of the tube (see Section 3.2.3). This will allow a shorter focus coil which results in the power savings.

The design goal of 3 watts in the sensor can be met. To accomplish this would require repackaging the high voltage supply, the focus control and both deflection controls in the electronic control unit and modifying the present focus coil. A breakdown of the new sensor power estimate is given in Table 2.4.2-1.

2.4.3 SATURATION RECOVERY TIME

The EPEM can comply with the 0.5 sec. recovery time, but can only partially comply with the 0.1 sec. recovery time. The lock-on time of the EPEM varies from approximately 0.16 sec. to 0.3 sec., and is dependent on many factors, several of which are beyond the control of the subsystem. The erase cycle is presently 0.065 sec., but may be reduced depending on the outcome of future trade-off studies. The write cycle varies from approximately 0.01 to 0.150 sec., depending on scene brightness. There is an additional 0.080 sec., approximately, required for lock-on stabilization.

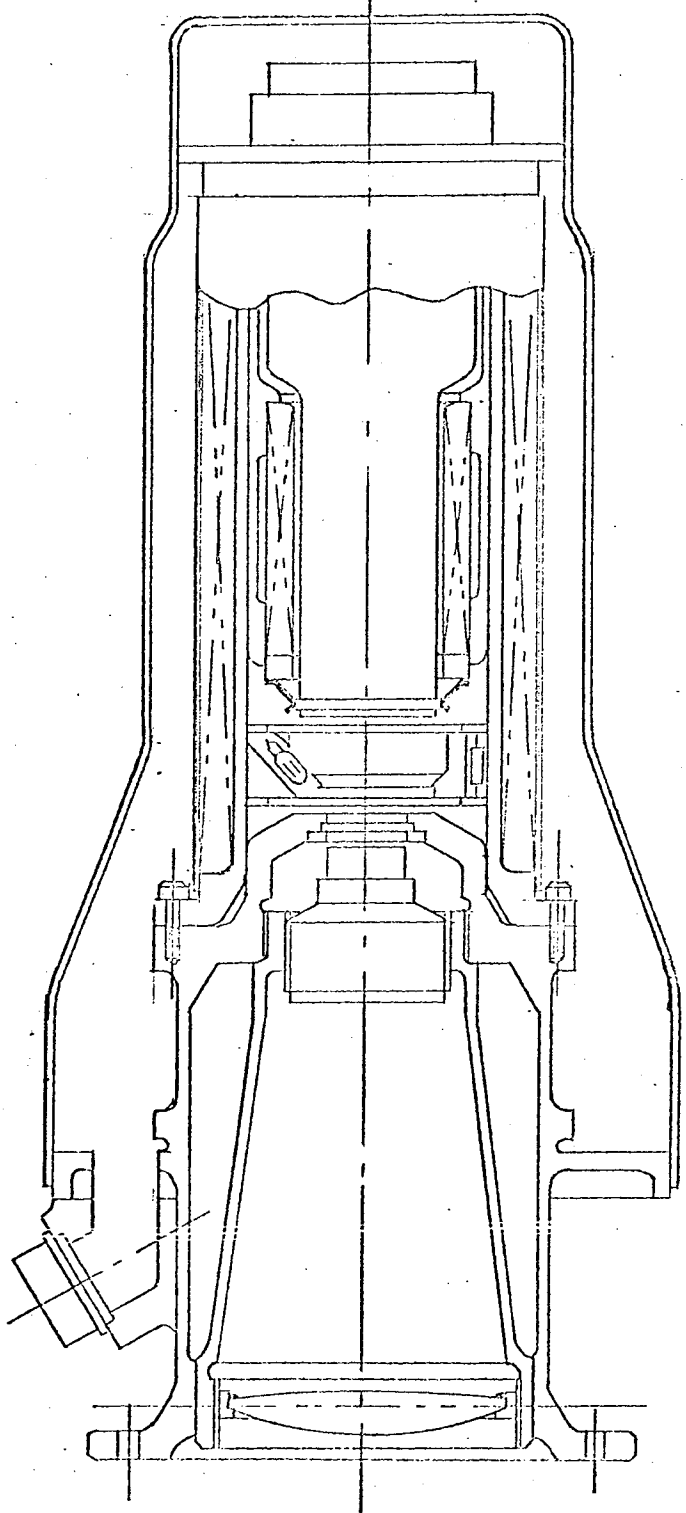

Figure 2.4.1-2. Proposed Sensor Assembly Incorporating Adapter and Short Tube

~~SECRET/D~~

TABLE 2.4.2-1 - SENSOR MINIMUM POWER ESTIMATE

COMPONENT	POWER (WATTS)
CORRELATRON	0.120
DEFLECTION COIL	0.049
FOCUS COIL	1.856
ERASE LAMPS	0.080
ERASE LIGHT CONTROL	0.081
H.V. CONTROL	0.730
BUFFER AMPLIFIER	0.042
CATHODE MONITOR	0.042
TOTAL	3.000

When a disable signal is not supplied to the BETA Subsystem, but it is saturated, the subsystem will continuously recycle until it locks on. If the image velocity falls below the dynamic range of the BETA Subsystem during the last 0.1 sec. of the cycle, the requirement for 0.1 sec. recovery will be met. If the image velocity falls below the dynamic range of the BETA Subsystem during the rest of the lock-on cycle, the recovery time will be greater than 0.1 sec.

There will also be times when the subsystem will lock on for image velocities above 0.3 in/sec. If the tracking mirror can respond fast enough to prevent the live image from reaching the edge of the stored image, the recovery time of 0.1 sec. can be achieved.

It is possible to comply with the saturation recovery time of less than 0.1 sec. by use of an electronic anticipation circuit in which the rate of change of saturated image velocity will be detected and the recycle point determined such that the recycle time will be completed as the image velocity just comes out of saturation. This concept is feasible since the inner loop of the BETA Subsystem accurately tracks image velocities up to 0.5 IPS. However, an output rate saturation indication is provided when the indicated rate exceeds 0.3 IPS per the system requirements. A typical plot of image velocity vs. time for normal operating and saturation ranges is shown in Figure 2.4.3-1. Note that the image velocity rate of change would be detected such that as the rate decreases, the recycle point occurs at approximately 1.75 sec. which, with an assumed 0.25 sec. recycle time allows the BETA Subsystem to provide indicated velocities in the operating range at 2.00 sec. when the image rate reaches 0.3 IPS.

Use of the electronic anticipation circuitry whose operation would be based on rate saturation indication commands, cathode monitor voltage (to determine write time) and tracking mirror outer-loop response time limits would allow the saturation recovery time requirement of less than 0.1 sec. to be satisfied. The degree of circuit sophistication required, naturally, is dependent upon the characteristics of the image rate during the period when the rate exceeds 0.3 IPS.

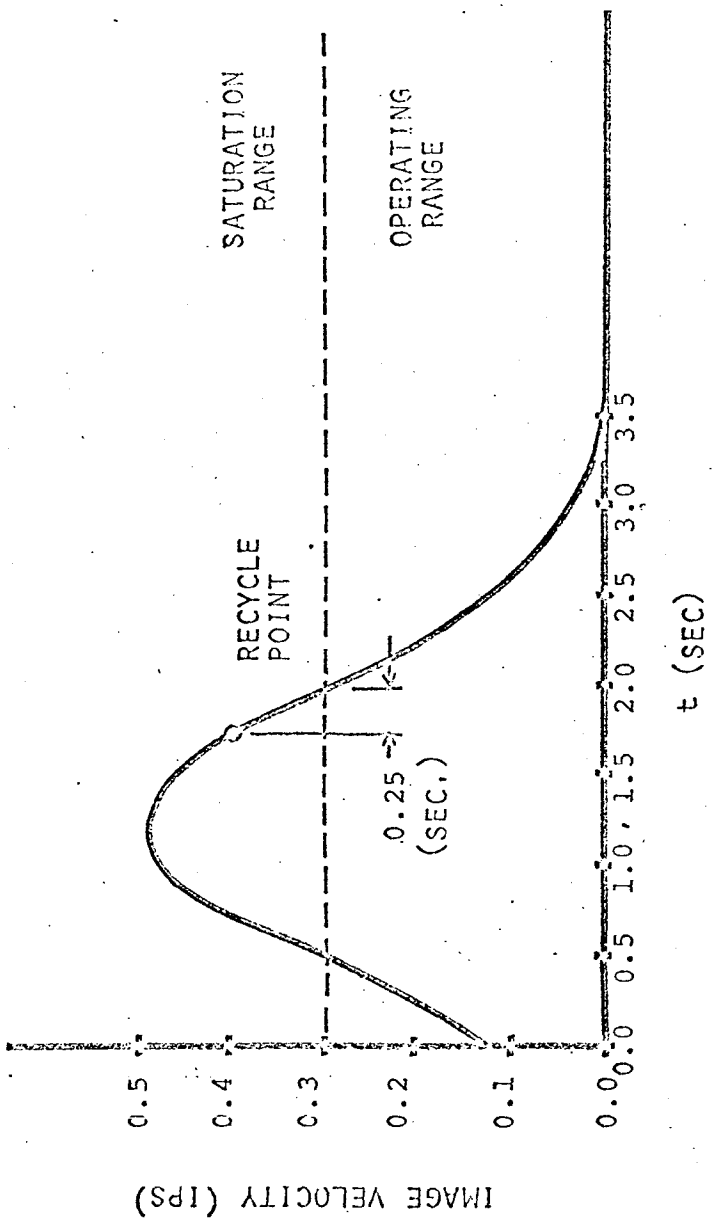

Figure 2.4.3-1. Saturation Recovery Time Example Using Electronic Anticipation Control

3.0 RELATED PROGRAM EFFORT

3.1 TECHNICAL STUDIES

The technical reports written during this program may be classified into three general categories. These are:

(1) BETA Subsystem Analysis & Performance Parameters,
(2) Storage Tube (Sensor) Operation & Parameters,
(3) Scene & Illumination Characteristics.

Titles of the studies undertaken on this program are shown in the Detail Milestone Chart (see Appendix A).

3.1.1 BETA Subsystem Analysis & Performance Parameters

Studies dealing with the BETA Subsystem performance parameters such as theoretical response, dynamic response vs. accuracy and length of track and accuracy as a function of line-of-sight were made as normal program documentation procedures. Also, analyses of the sensor stress and thermal characteristics were made to determine compliance with the program requirements.

An extensive study was made of cloud characteristics and the effects of clouds on the BETA Subsystem performance. Based on the operational theory of the system, a minimum number of signals were determined which would provide a reliable indication of cloud presence determined from the BETA Subsystem outputs.

As a result of testing performed on both BETA Subsystem breadboard models (Princess I and II), it was found that an unexplained indicated velocity for the in-track component was present for no apparent input image velocity as the stereo angle was varied through limits of +40° to -40°. This phenomenon, called the dynamic null output, was the subject of considerable investigation. Geometrical configurations for both real and simulated cases were defined and mathematical equations relating both image motion and shading at the BETA Subsystem optical interface as a function of stereo angle were derived. It was concluded that the apparent rates observed were

due to the target movements and image shading resulting from the shorter focal lengths (compared to the real-case focal length) used in both PAUL and M&M simulators. Good correlation between simulated measured rates and theoretical rates were obtained and it was further concluded that, for the scenes investigated, the corresponding apparent real-case image rates would be approximately 70 times less than produced in the M&M simulator and would be within the required specification limits for dynamic null accuracy. However, it is PAUL's opinion that further investigation is necessary in the area of dynamic null accuracy to evaluate the magnitude of apparent along-track velocities as a function of stereo angle over a wider range of scene parameter variations for the real-case conditions.

In order to evaluate the BETA Subsystem noise and bias errors accurately and with a minimum data reduction time, a method was developed which allows the rate output voltages to be transmitted to an analog-digital converter remote from the testing area. The digital rate information, contained on magnetic tape is then processed by an IBM 360 digital computer and power spectral density print-outs and computer-derived PSD plots are made. The PSD program, developed specifically for this program, involves the use of the Fast Fourier Transform which significantly reduces the computation time while allowing the accuracy of the PSD evaluation to be increased and allowing easy removal of any periodic frequencies present.

3.1.2 SENSOR TUBE OPERATION AND PARAMETERS

As part of the Performance Prediction Techniques study, it was necessary to formulate a realistic mathematical model of the sensor tube in order to predict the overall sensor performance as a function of changes in the input image characteristics or of changes in the sensor parameters.

The sensor tube internal operations leading to an electrical output signal are combinations of four basic physical phenomena, for which the defining mathematical representations were first derived. These model elements - photoemission, electron image focusing, storage mesh surface dynamics, and storage mesh transmission - were then related by additional mathematical formulae which define how the model elements interact to produce the tube output scene. These formulations, referred to as synthesis operations, were made so as to provide the capability of being incorporated into an integrated tube model consistent with the mathematical concepts used to describe the input scene parameters.

3.1.3 SCENE AND ILLUMINATION CHARACTERISTICS

The performance capability of the sensor is a function of the quality and quantity of the image information presented to the sensor, and is also a function of the ability of the sensor to utilize this information. The image input information is not constant and is dependent on a variety of localized changes within the image format which include: illumination level, color, contrast, focus, scale and geometrical orientation. Accordingly, the scene and illumination characteristics of the input image were the subjects of considerable investigation during this program to obtain engineering data relating to:

(1) Determination of which input image parameters influence the PAUL sensor performance,

(2) Determination of how the significant input image parameters should be specified,

(3) Development of a mathematical model of the input image parameter specifications which would be a compatible forcing function for the related mathematical model of the sensor transfer function.

The approach used to obtain the required engineering data was to initiate studies which would allow the isolation and control of specific image parameters. This was accomplished by defining, generating and evaluating synthetic images derived from a digital computer. The generated synthetic imagery allowed the scene information content to be quantized and minimized to the extent that all the information contained could be controlled and completely specified. With a controlled method of generating synthetic images thus available, the analytical effects of scene parameters such as scale, azimuth, contrast, spatial frequency, orientation, color, focus and target distribution were analytically evaluated by a computer correlation of the basic X,Y scene parameters. Comparison of correlation (matching) results obtained using photographs of the synthetic map and a PAUL sensor tube allowed the analytical match curves to be compared to laboratory results for the controlled parameters.

Additional studies were made concerning spectrum utilization to demonstrate the improvement in the BETA sensor low light level sensitivity which could be obtained by a modification of the spectral transmission characteristics of the Main Optics Assembly. Since the incoming available optical energy extended considerably beyond the restricted band provided for the Camera Assembly image, the studies were undertaken to demonstrate that the PAUL sensor could utilize a portion of this additional energy and thus significantly improve the low-light capability of the BETA Subsystem. Necessary analyses of factors which influence the spectral content of the image such as geometry, atmospheric absorption, reflectance, etc. were made. In addition, an analysis of the transmission properties of the PAUL sensor optics and spectral conversion efficiency of the sensor photocathode was required to evaluate the sensor response to the incoming optical parameter variations.

3.2 SENSOR TUBE CONFIGURATION AND POSSIBLE IMPROVEMENTS

3.2.1 GENERAL

This section discusses modifications made to the sensor tube during the program and possible future modifications which would enhance the performance and/or reduce size, weight, and power. Details on the tubes procured may be found in section 3.2.2. In the future, the possibilities are divided into: (1) reduction of the tube size which could be easily accomplished, and (2) configurations that are being investigated under PAUL corporate R&D that will enhance the sensor tube capabilities in one or two years.

3.2.2 PRESENT CONFIGURATION

The model 190X tube used in the EPEM is specified in PAUL SCD 623A500-308-103. At the start of the program, the tube model specified was the 395. This model differed from the 257 model of the previous program on the following:

(1) Minimum photocathode sensitivity of 2 of the 395 tubes was 180 μa/lumen and of 4 tubes was 200 μa/lumen compared to 150 μa/lumen of the 257 model.

(2) Connection to the base of the 395 was with pigtail leads and the base was potted compared to the connector used on the 257 model.

Concurrent with the start of the 395 program, the tube vendor proposed using unencapsulated resistors in the internal electron multiplier bleeder. This would increase yield because of the possibility of a leak in the capsulated resistors. Tubes were provided to PAUL for performing life and environmental test. After passing these tests, the 4 - 200 μa/lumen 395 were changed to unencapsulated resistors.

As the program progressed, it became apparent that the low light level/contrast capabilities of the tube required improvement. This, in essence, required that the write exposure of the sensor tube be reduced. Therefore, a program was initiated to:

(1) reduce the storage mesh capacitance by increasing the dielectric thickness by a factor of 2,

(2) increase the front end transmission by using a high electron transmission collector mesh.

These modifications were successful and resulted in a model 190 tube. Measurements on four 190 tubes showed a reduction of 2.4 to 4.0 in the write exposure. In addition, the 190 tubes had cesiated electron multipliers which reduced the multiplier fatigue.

At this time, another problem developed when the available input illumination was increased. While the write time was reduced, during the read mode the electron multiplier could saturate. Saturation was due to inadequate bleeder current and was solved by bringing dynodes 7, 8, and 9 (in addition to 1 and 10) out of the tube. Thus an external divider could be used for the last stages which resulted in an order of magnitude increase in anode current before saturation occured.

The above modification and results are summarized in Table 3.2.2-1.

TABLE 3.2.2-1 - SENSOR TUBE MODIFICATIONS

Sensor Tube Model No.	Change from Previous Model	Results
257	Tube used on previous program	-
395	(1) pigtail leads and potted base	(1) increased reliability
	(2) increased photocathode sensitivity	(2) improved low light/ contrast operation
	(3) unencapsulated resistors	(3) increased yield
190	(1) thick dielectric (2) high transmission collector mesh	(1) & (2) improved low light/contrast operation
	(3) cesiated electron multiplier	(3) reduced multiplier fatigue
190X	Dynodes 7,8 and 9 brought out	Eliminated multiplier saturation at high illumination

3.2.3 FUTURE IMPROVEMENTS - MINIMUM MODIFICATIONS

The following changes are possible in order to improve the configuration of the sensor:

(1) The tube length may be reduced by 1.4 inch in the photocathode to storage mesh spacing. This has been verified on an Air Force guidance program in which the shorter length tube is used.

(2) The electron-multiplier length may be reduced by 0.9 inch without any changes internal to the tube.

(3) Because of the reduced electron multiplier fatigue with cesiation, two or three dynode stages may be eliminated. The reduced length would be 0.15 inch per dynode eliminated.

Thus the length may be reduced by 2.3 inches plus 0.15 inch per stage of multiplier gain eliminated. Also, the storage mesh dielectric thickness may be increased by another factor of 2. Two tubes of

this nature are currently under evaluation by the tube manufacturer and show a reduction of greater than 4 in the write exposure as compared to the 395 model. The modification would require additional evaluation before incorporation into a final design.

3.2.4 FUTURE IMPROVEMENTS - ONE TO TWO YEARS

Under PAUL Corporate R&D, modifications to the tube to improve its capabilities are being investigated. The improvements applicable to the sensor could be incorporated in one to two years, depending upon the R&D progress and contractual funds for ruggedization and life verification. The items considered applicable to the sensor are as follows:

(1) Use of a micro-channel plate electron multiplier in place of the dynode multiplier is under investigation. This would reduce the tube length to less than 6 inches.

(2) With the micro-channel plate multiplier, a many segmented anode could be used for cloud discrimination and tracking only to cloud free areas.

(3) An electrostatically focused and deflected tube is under investigation. This tube would be approximately 1-1/2 inches in diameter by 4 inches long. In addition, the sensor power and weight would be reduced due to elimination of the focus and deflection yokes and the sensitivity would be doubled due to elimination of the field mesh.

In addition, it is estimated that the minimum S25 photocathode sensitivity of 250 μa/lumen will be possible in one year and will reach an anticipated maximum value of 300 μa/lumen in two to three years.

3.2.5 LIFE TESTS

3.2.5.1 TUBES

The electrical performance of several sensor tubes, subjected to typical operating conditions, was measured in a series of tests performed on the PAUL life tester. The life tests and their durations for each tube tested are shown in Table 3.2.5-1.

TABLE 3.2.5-1 LIFE TESTS TABULATION

Tube	Life Test	Duration (Hrs.)
066802-2	1	1177.8
036801-LT-31	1	1165.0
	2	2445.2
TOTAL		3610.2
076703-8	1	1149.2
	2	1280.7
	3	1134.0
	4	1165.0
TOTAL		4728.9
086702-11	1	1149.2
	2	1185.4
	3	1134.0
	4	1263.3
TOTAL		4731.9

3.2.5.2 TEST CONDITIONS

All tubes were automatically cycled every three (3) seconds, and with the exception of evaluation testing time, the tubes were cycled twenty-four (24) hours a day, seven (7) days a week.

The performance effect of different voltage combinations on the tube elements was observed during the life tests.

3.2.5.3 RESULTS

Results of life tests performed on four tubes are shown in Table 3.2.5-2. Photocathode sensitivity and multiplier gain decay or increase is expressed in percentage for each test. The type of decay or increase is noted for each test and is expressed as either exponential decay, gradual decay, or where no definite pattern was evident, was expressed as random.

3.2.5.4 SUMMARY

All life tests with the exception of life test No. 1 on 036801 LT-31 and life test No. 4 on 076703-8 were performed using tube potentials near those used in the BETA Subsystem (20 volts on field, collector and drift tube elements). No failures were experienced during the life tests. The rapid drop-off in multiplier gain during the first life test of each tube is considered normal and did not affect the operation of the tube as determined from evaluation tests performed after each life test run.

Two life tests were performed as noted above to determine the effects of second node operation in which the field mesh, collector mesh and drift tube were held at 190 Volts. Operation in this region causes severe ionization which accounts for the excessive drop in cathode sensitivity. Because of this, second node operation cannot be considered satisfactory for BETA Subsystem operation although a theoretical increase in tube resolution is possible for second node operation which was the basis for life testing under these conditions.

A comparison between the type using a cessiated electron-multiplier (LT-31) and tubes with non-cessiated multipliers showed that significantly less decrease in multiplier gain was obtained with the LT-31 tube. The sensor tube used in the EPEM contains a cessiated electron-multiplier section in order to minumize multiplier gain decrease.

TABLE 3.2.5-2 TABULATED LIFE TEST RESULTS

TUBE	LIFE TEST	CATHODE SENSITIVITY	COMMENTS	MULTIPLIER GAIN	COMMENTS
F68-190 066802-2	1	12.71% Drop	Gradual Decay	27.2% Drop	Exponential Decay
036801 LT-31	1 *	72.4% Drop	Approximately Exponential Decay	4.2% Drop	Exponential Decay to 2600, then Rise to 4100
	2	1.82% Rise	Random	21.95% Drop	Exponential Rise to 5840, then Decay to 3200
076703-8	1	10.81% Drop	Random	74.0% Drop	Exponential Decay
	2	1.61% Drop	Random	2.38% Rise	Exponential Rise to 193, then Random Decay to 172
	3	3.86% Rise	Random	No Change	-
	4 *	34.9% Drop	Random	7.56% Rise	Random
086702-11	1	6.54% Drop	Random	86.5% Drop	Exponential Decay
	2	6.97% Rise	Random	9.64% Drop	Random
	3	6.20% Drop	Random	16.0% Drop	Random
	4	5.07% Rise	Random	9.10% Drop	Random

* Second node operation

4.0 ANCILLARY TESTER

4.1 DESCRIPTION

As required in Paragraph 1.3 of Reference 1, the Ancillary Tester was designed and built to support on-site engineering testing of the Engineering Prototype Evaluation Model.

The Ancillary Tester allows a variety of testing functions to be performed on the EPEM including:

(1) Signal monitoring,
(2) Signal interrupt and injection,
(3) Open and closed-loop operation,
(4) System hold condition in pre-selected operational modes,
(5) Trouble-shooting.

The EPEM system status can be continually monitored from meter readings and indicator lamp status as observed on the Programmer front panel.

The Ancillary Tester consists of the following equipment:

(1) Programmer,
(2) Two signal monitoring boxes designated as Break-Out and Input-Output boxes,
(3) Nine interconnecting cables.

Figure 4.1-1 shows the available interconnections between the Ancillary Tester and the EPEM. Several variations are possible depending on which combination of signal monitoring boxes, programmer and associated cables are used.

4.2 OPERATION

4.2.1 PROGRAMMER

The BETA Subsystem operation and monitoring is controlled from the Programmer front panel switches, indicator lamps and meters.

Functionally, the Programmer controls and monitors may be classified as follows:

(1) Input Control,
(2) Output Control and Monitoring,
(3) Internal Testing Control,

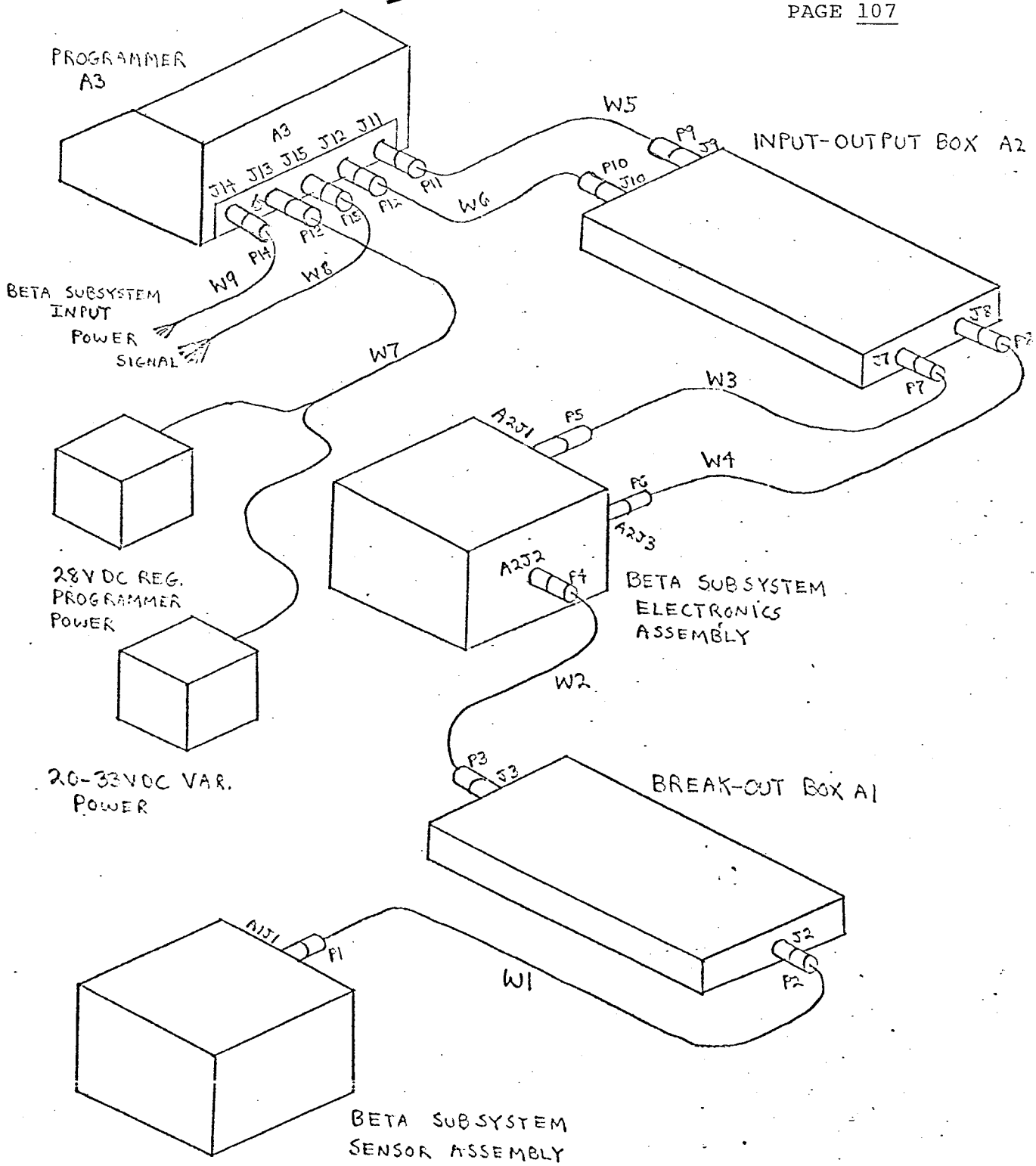

Figure 4.1-1. Interconnection of Ancillary Tester and EPEM

4.2.1.1 INPUT CONTROL

All input control commands are generated internally within the Programmer while inhibiting the normal input commands to the BETA Subsystem. Input commands are:

(1) Master Power,
(2) Operate Command,
(3) Track Command,
(4) Inhibit Command.

4.2.1.2 OUTPUT CONTROL AND MONITORING

The output control and monitoring functions may be listed as:

(1) Recycle,
(2) Cathode Current Meter,
(3) X and Y Rate and Position Meter,
(4) X and Y Polarity Bits,
(5) X and Y Rate Saturation,
(6) Lock-on,
(7) Subthreshold Illumination,

4.2.1.3 INTERNAL TESTING CONTROL

Several Programmer control switches and indicators are provided for the purpose of BETA Subsystem internal testing control while analyzing system performance during testing and trouble-shooting. The purpose of the internal testing control switches is to allow the BETA Subsystem to be held in any desired mode for as long as required. Additionally, manual cycling and single-axis operation are available. The internal testing controls are:

(1) Standby Mode Lock,
(2) Erase Mode Lock,
(3) Manual Erase,
(4) Write Mode Lock,
(5) Verification Mode Lock,
(6) Clock Stop and Manual Clock,
(7) X and Y Nutation Inhibit.

4.2.2 SIGNAL MONITORING BOXES

The two signal monitoring boxes allow access to all signal and power lines from the associated connectors. Access to any line is obtained by the use of top-mounted banana jacks and shorting plugs. Any line may be disconnected for signal injection or current measurements by removing the shorting plug.

The Input/Output (I/O) box, when used, is connected either (1) between the EPEM electronics package and input cabling, or (2) between the electronics package and Ancillary Tester Programmer with input cabling connected to the Programmer.

The Break-out (B/O) box, when used, is connected between the electronics package and Sensor Assembly of the EPEM.

APPENDIX A
DETAIL MILESTONE SCHEDULE
PART O
(PAUL)

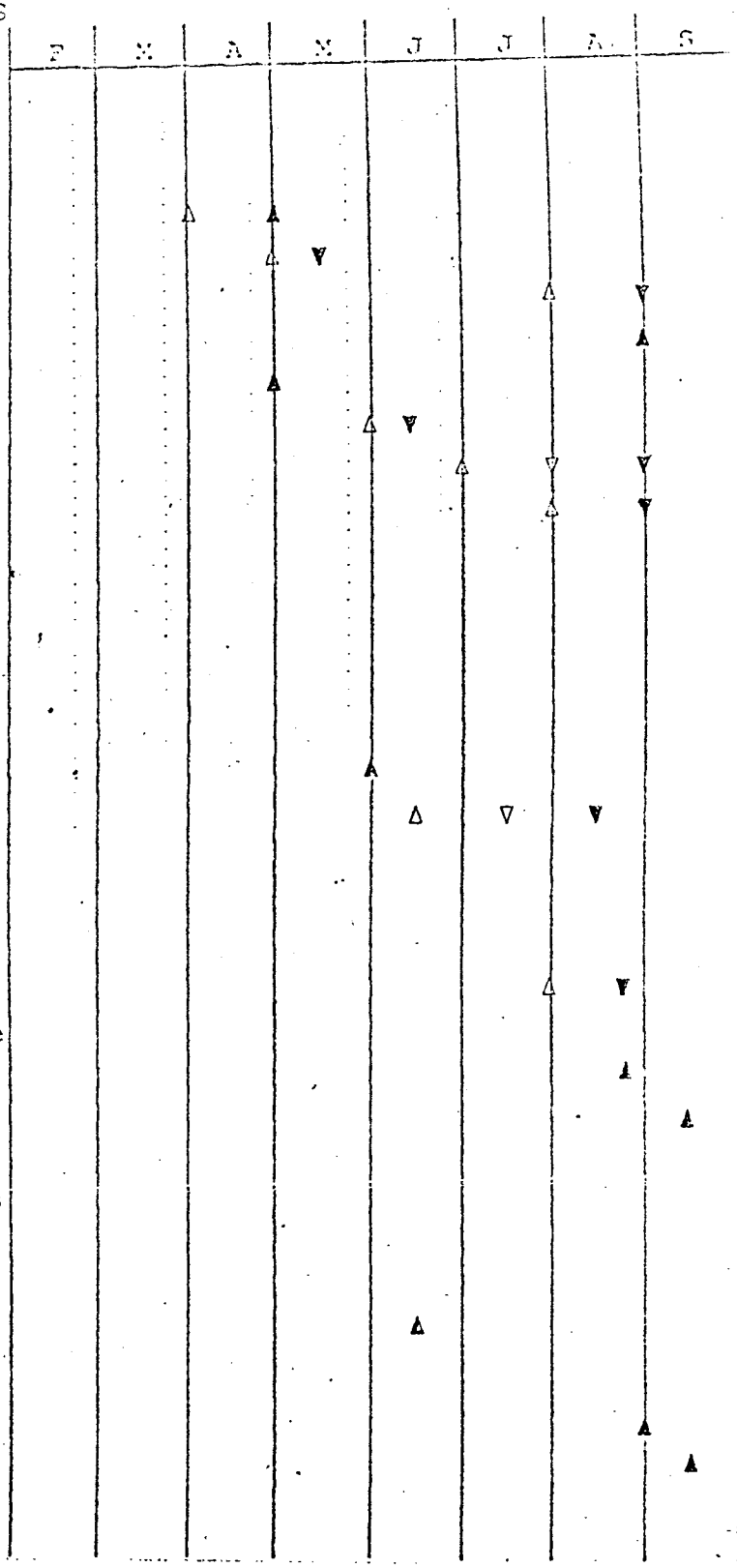

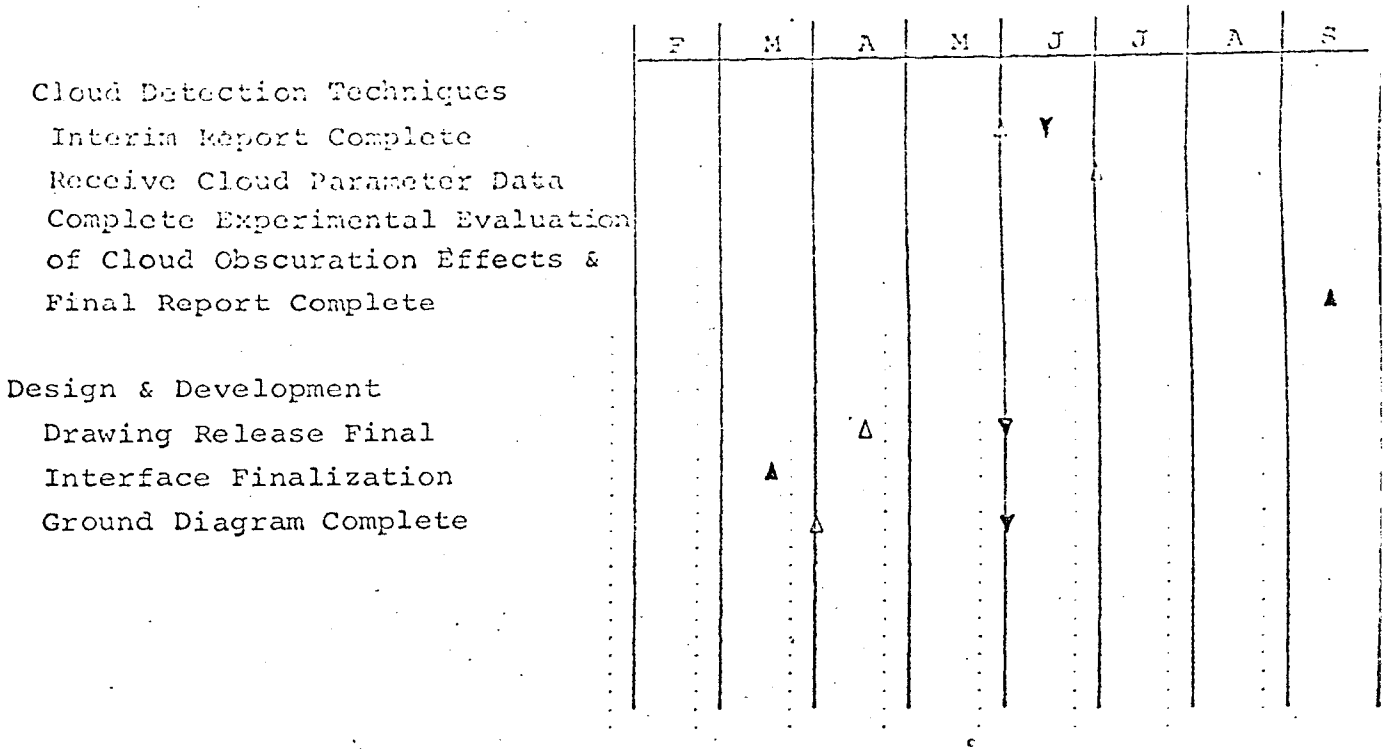

SECRET/D

1.2 ENGINEERING HARDWARE

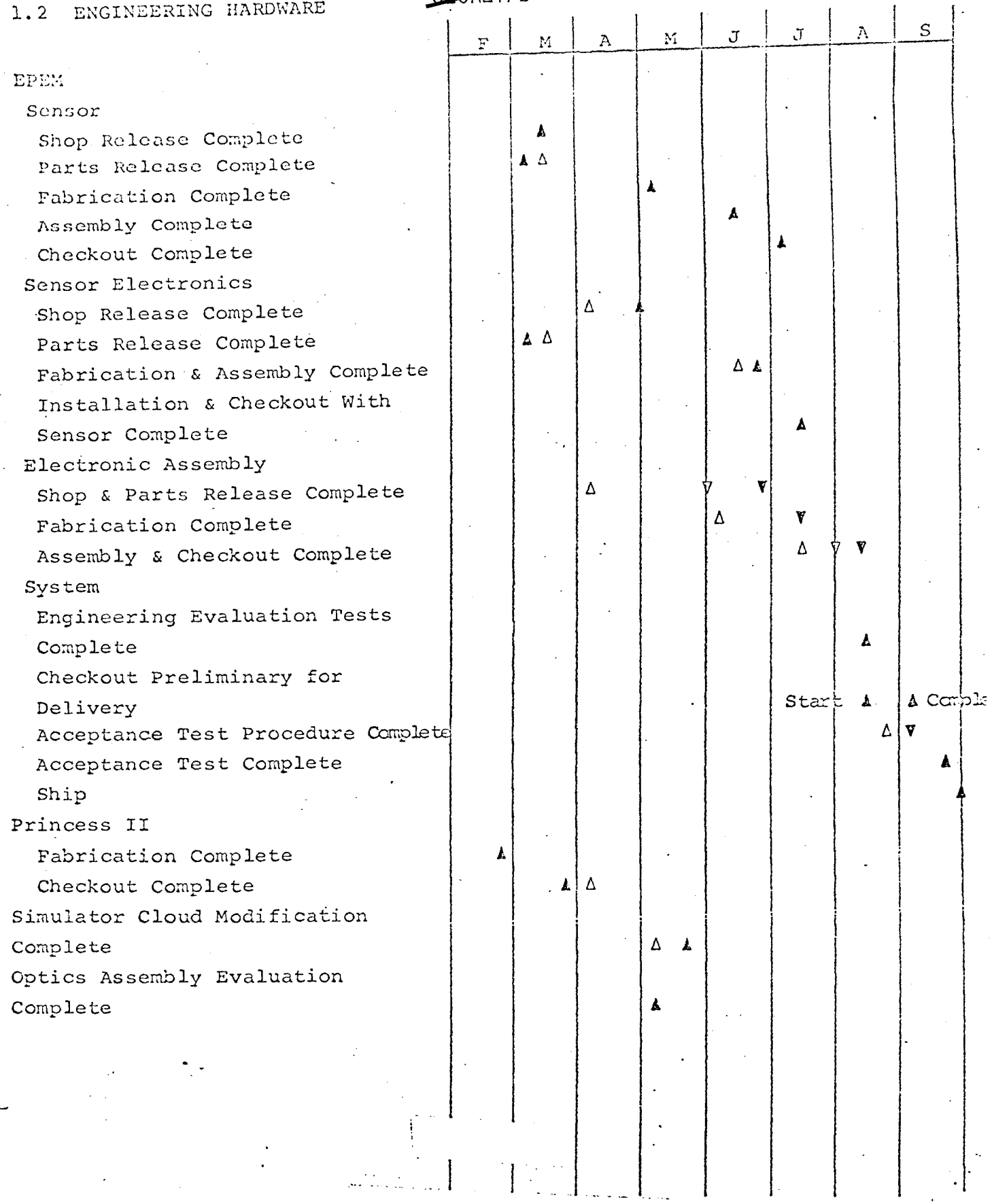

SECRET/D

1.3 GENERAL ELECTRIC SUPPORT

Ancillary Tester
- Design Complete
- Fabrication Complete
- Assembly Complete

- Fab. New Control Box Complete
- Checkout Complete
- Procedure Complete
- Ship

4.0 MANAGEMENT & ADMINISTRATION

- Status Reports
- T/D Meetings
- Cost & Manpower Report
- Detail Milestone Schedule

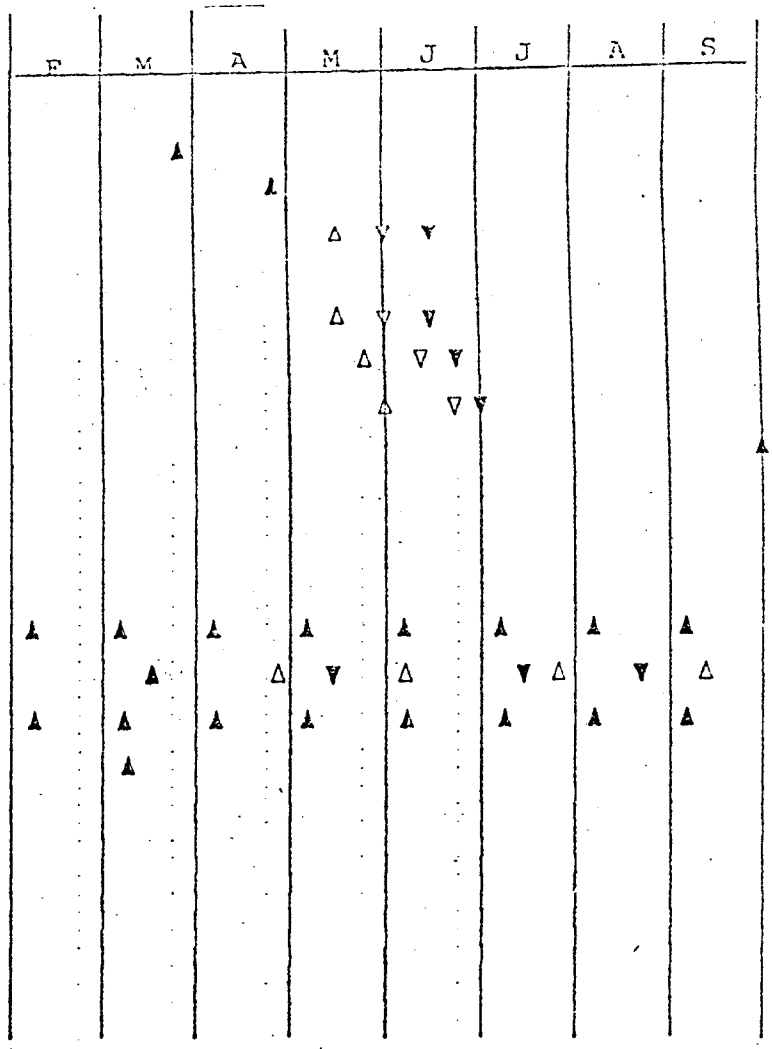

LEGEND:

Δ = Scheduled Milestone

▲ = Completed Milestone

∇ = Rescheduled Milestone

APPENDIX B - FUNCTIONAL DIFFERENCES BETWEEN EPEM AND BETA BREADBOARD MODEL (PRINCESS I)

FUNCTION	BREADBOARD UNIT (PRINCESS I)	EPEM
Output Rates	Bi-Polar Analog	Single Polarity Analog with Digital Polarity Indicator
Diagnostic Monitoring	Analog Outputs with Zero Volt DC Reference	Analog Outputs with +2.5V DC Reference - Outputs Limited Between Zero and +5V DC
Nutation Diameter Controlled by Nutation Generator	Fixed Diameter	Variable Diameter
Automatic Recycle Time	6 Sec.	2 Sec.
Signals Indicative of Clouds	None	4 IOC Output Lines
A.G.C. Circuit	Separate X and Y F/B Control	Multiplexed Single Channel F/B Control
Rate Saturation Indicators	None	X and Y Indicators
Demodulator	Separate X and Y Demodulators	Multiplexed Single Stage Demodulator

SECRET/D